Effect of Encapsulation Materials on Tensile Stress during Thermo-Mechanical Cycling of Pb-Free Solder Joints

Maxim Serebreni, Dr. Nathan Blattau, Dr. Gilad Sharon, Dr. Craig Hillman
DfR Solutions
Beltsville, MD

Abstract
Electronic assemblies use a large variety of polymer materials with different mechanical and thermal properties to provide protection in harsh usage environments. However, variability in the mechanical properties such as the coefficient of thermal expansion and elastic modulus effects the material selection process by introducing uncertainty to the long term impacts on the reliability of the electronics. Typically, the main reliability issue is solder joint fatigue which accounts for a large amount of failures in electronic components. Therefore, it is necessary to understand the effect of polymer encapsulations (coatings, pottings and underfills) on the solder joints when predicting reliability. It has been shown that there is a large reduction in fatigue life when tensile stresses exist in the solder due to the thermal expansion of the polymer encapsulation. The inclusion of tensile stress subjects solder joints to cyclic multiaxial stress state which is found to be more damaging than a conventional cyclic shear loading. Isolating the tensile stress component is necessary in order to understand its influence on a reduced fatigue life of microelectronic solder joints. Therefore, a unique specimen was constructed in order to subject Pb-free solder joints to the fluctuating tensile stress conditions. This paper presents the construction and validation of a thermo-mechanical tensile fatigue specimen. The thermal cycling range was matched with potting expansion properties in order to vary the magnitude of tensile stress imposed on solder joints. Solder joint geometries were designed with a scale factor that is relevant to BGAs and QFN solder joints while maintaining a simplified stress state. FEA modeling was performed to observe the stress-strain behavior of solder joints during thermal expansion for various potting material properties. The magnitude of axial stress in solder joints is shown to be dependent on both the coefficient of thermal expansion and modulus along with the peak temperature of thermal cycles. Results from thermal cycling of the specimen assist in correlating the magnitude of tensile stress experienced by solder joints due to the thermal expansion of potting material with various expansion properties and provides new insight into low cycle fatigue life of solder joints in electronic packages with encapsulations.

Introduction
A large amount of failures in electronic components are attributed to solder joint fatigue failure. Many electronic components in aerospace, automotive, industrial and consumer applications operate under fluctuating temperatures which subject solder joints to thermo-mechanical fatigue (TMF) conditions. Solder fatigue in electronic assemblies is the culmination of both fluctuating temperature and coefficient of thermal expansion (CTE) mismatch between components and printed circuit boards (PBCs). During temperature change, the difference in CTE of the PCB and components causes a differential material expansion which in turn places solder joints under shear loading. To reduce the shear strain imposed on solder joints in chip scale packages (CSPs) various underfill materials are used to limit the deformation of solder joints. Die level solder interconnects such as in flip chip packages in particular benefit from underfill by redistributing thermal expansion stresses and thus limiting the strain imposed on solder bumps. In addition to limiting shear strains, underfill expansion has been shown to cause large normal strains in ball grid array (BGA) solder joints. Kwak et al. used a 2D DIC technique with optical microscopy to measure strain in solder joints subjected to thermal cycling [1]. They found that an underfill with CTE of 30 ppm/ºC and a glass transition temperature (T_g) of 80ºC can generate an average normal strain of 6000 με at a temperature of 100ºC. These high normal strains do not show the same dependence on distance to neutral point as shear strains do in BGA packages. The magnitude of normal strain has a complex dependence on the CTE, elastic modulus (E), package size and temperature. The addition of normal strains places solder joints under a combination of shear and axial strains which in turn subjects solder joints to non-proportional cyclic loading during fluctuating temperature conditions.

To limit the large axial strains, low CTE underfill should be selected to reduce the local mismatch. Previous studies have shown that when underfill CTE closely matches the CTE of the solder, package reliability can be extended by a factor of 2 compared to non-underfill components [2]. Current numerical investigations predict that the addition of certain underfill materials should extend the life of BGA solder joints far more than is proven by experiments. The reason in deviation from the experimental data is the misinterpretation of the stress and strain state to the contribution of damage parameters in existing fatigue life models. During underfill expansion, a mean tensile or compressive stress can be added to the existing shear strains. Addition of a positive tensile stress has been shown to drastically reduce the fatigue life in cyclic experiments on bulk lead-free solder. Liang et al. performed torsional fatigue experiments with axial constant stress on SAC305 solder and found that the addition of a 6 MPa constant axial stress to cyclic shear loading reduced fatigue life by a factor of 14 at 0.34% shear strain range and a factor of 4 for 3.46% shear strain range [3]. The fatigue life of SAC305 at room temperature is shown to have a power relationship with ratcheting strain rate and the inclusion of even low axial stress or strain can cause high ratcheting strain which drastically reduce time to failure [4]. At high temperatures, a ratcheting breakdown phenomenon

can occur in which ratcheting strain is no longer accumulated due to the cyclic creep behavior of solder. The exact temperature at which ratcheting breakdown occurs in solder alloys has not been investigated and its influence on TMF life is not known. In addition to uncertainty on the influence of temperature on ratcheting strain in Pb-free solder, fatigue properties could also vary due to the difference in size dependent microstructure of bulk and macroscale solder joints. Andersson et al. performed isothermal fatigue experiments on bulk and macroscale solder joints and observed an inverse fatigue life performance at low and high strain ranges [5]. A significant factor that could have manipulated results from their study was the type of strain used in cyclic experiments. Bulk solder was tested in cyclic tension/compression and solder joints were tested under cyclic shear loading. It is known that fatigue crack propagation rates in solder alloys are dependent on the geometry, intermetallic layer thickness and loading mode [6].

In order to evaluate the axial stress contribution to the reliability of solder, the fatigue life of solder joints under purely axial loading mode needs to be investigated. To experimentally subject macroscale solder joints under TMF conditions by means of purely axial loading a new test coupon was devised. The test coupon consists of placing a grid of solder joints in between two PCBs to avoid potential shear strains and use potting materials to facilitate axial displacement during thermal expansion. Since space between the two PCBs is designed with significantly larger gap compared to that in CSP, the encapsulant used to fill the gap were not limited to just underfill materials.

This paper presents the development process of a test specimen designed to reproduce the CTE mismatch driven tensile loading caused by material expansion during thermal cycling. The specimen is intended to induce axial loading driven by CTE mismatch of materials. A step-by-step construction procedure of the specimen is presented along with associated design iterations made to enhance the intended function. To correlate the magnitude of stress and strain solder joints experience, an analytical displacement compatibility equation was used to select the appropriate thermal cycling range for each potting material. Potting materials with various glass transition temperatures (T_g) were selected to evaluate the stress on the solder when thermally cycles across their range in comparison to potting materials with thermally stable behavior. Finite element modeling was used to capture the deformation in solder joints and correlate stress-strain state to potting material properties at various temperatures. Experimental results could be used in understanding the contribution of axial loading on TMF life of solder joints in encapsulated assemblies.

Material Selection

To vary the stress level with temperature it is desirable to control both the CTE and E of potting materials. The selected materials are commercially available thermoset epoxies, acrylics and polyurethane used as pottings, underfills, conformal coatings and general encapsulants in electronic products. Six materials were initially selected with various properties as shown in Table 1, and are provided by the manufacturers. Materials with a range of T_g and hardness values were selected along with different combinations of CTE and E.

Table 1 Potting material coefficient of thermal expansion and modulus

Material ID	PM1	PM2	PM3	PM4	PM5	PM6
E (GPa)	1.02	2.81	0.16	0.34	10.7	2.5
T_g (ºC)	35	145	-50	-2	130	120
CTE<T_g (ppm/ºC)	77	37	N/A	N/A	28	44
CTE>T_g (ppm/ºC)	195	N/A	340	87	83	N/A
Shore Hardness	84D	90D	56A	88A	91D	89D

Epoxy potting materials show high coefficient of thermal expansion (CTE) at temperatures above their glass transition temperature (Tg). When low CTE epoxies are heated past their T_g, the large expansion could subject solder joints to excessive bending and normal stresses and lead to accelerated failure of components [7]. This is caused due to rapid increase in the CTE as the material approaches its glass transition temperature with no corresponding decrease in modulus. This delay arises since the CTE of polymers is driven by change in the free volume, while changes in the modulus are driven by increase in translational and rotational movements of the polymer chains.

Dynamic Mechanical Analyzer (DMA) and Thermal Mechanical Analyzer (TMA) analysis were conducted on potting material PM1 to obtain the T_g, Elastic modulus (E), and CTE. Figure 1 shows the rapid change in E and CTE of the material around the glass transition temperature. The data shows that the actual material CTE could differ by as much as 400% throughout a standardized test temperature profile. Particular note of importance to mention is that the manufacturer provided E and CTE values are taken as an average over a temperature range. Selection of potting materials without consideration to their glass transition temperature and intended operating temperature can increase the stress in solder joints and reduce component reliability by 20% or more [8].For potting materials with high T_g, a durometer was used to determine material hardness at a temperature range below the T_g. Consisted hardness values were found at desired test temperatures and substantiate the thermal stability of material properties below the T_g.

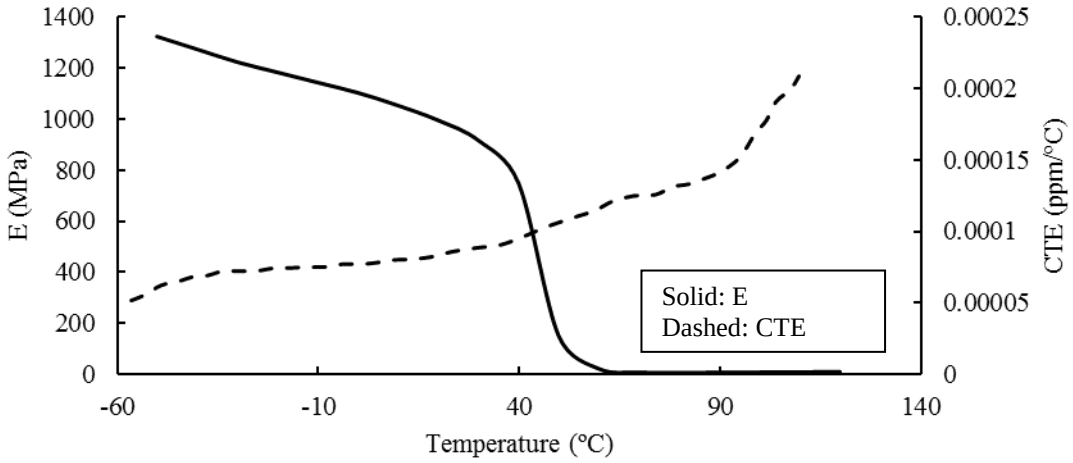

Figure 1 CTE and E versus Temperature characterization of potting material PM1

Coupon Design

The purpose behind creating the specimen stems from the inherent nature of CTE mismatch driven TMF. Testing different component sizes with various underfill material properties only alters a few test parameters but does not offer a true control of the extrinsic factors affecting fatigue life of solder joints. Since shear strain will always be present in testing, an alternative testing approach is proposed that is focused on eliminating the global CTE mismatch of PCB and component by placing a PCB on the top and bottom surfaces around the solder joint. Two of the most important parameters affecting the stress level in chip scale tests with underfill are the standoff height of reflowed solder spheres and component size. In order to have control on the stress or strain level, the specimen is designed with an adjustable standoff height as shown in Figure 2. The standoff height is controlled via through-hole solder joints that are attached to the upper PCB with the lower PCB connected using surface mount solder joints. Brass terminal pins are selected as interposers between the PCB and solder joints. The potting material is filled in the gap between the two circuit boards and around the solder joints and pins.

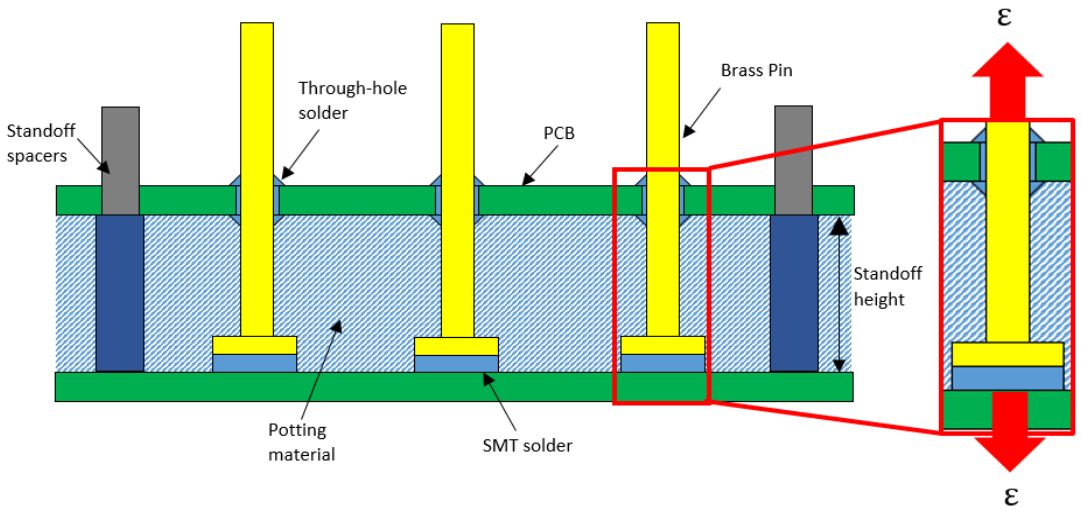

Figure 2 Illustration of specimen configuration

The PCB design is a double-sided two layer board with non-solder mask defined pads and OSP surface finish. Board thickness is 1.6mm. Spacing between surface mount pads is 6.35 mm. The full length and width of the specimen was 89mm and 25 mm respectively. Traces are routed to each through-hole joint and all surface mount pads were routed to common ground. The PCB is designed in order to be able to use a single board design for both sides of the specimen to reduce manufacturing cost and complexity. Surface mount pads and plated through-holes were placed interchangeably in three rows of eleven pins in each row. Four 4.3 mm diameter holes are drilled in each corner to provide fastening for standoffs

connectors. Standoff height is used to regulate the amount of potting filled in the space between the two boards. Surface mount solder joints are printed with SAC305 solder paste using 5 mil thick framed stencil. Through-hole joints are manually soldered using SN96 solder wire.

Nail head type brass terminal pins were used to connect SMT solder joints to the through-hole connections and provide a rigid interface during potting expansion. Brass pins have an overall length of 16.87mm with a flange diameter of 1.50mm. To prevent wetting of the solder paste along the sides of the gold plated flange during reflow, a 400 grit sand paper is used to remove the gold finish layer directly perpendicular to the mating surface. Sanding the flange sides removed the gold surface finish exposing the undercoat nickel layer while maintaining the gold finish on the bottom surface for reflow. Assembly procedure of the specimen is developed with a few number of steps to minimize error and maintain consistency and reproducibility as shown in Figure 3. The first step consisted of aligning a locking plate for the pin flanges. The locking plate is made from the same PCB with its surface mount pads drilled to match the diameter of the pin flange. A layer of polyimide tape is then placed underneath the fixture pad facing upward. This helps in securing the flange bottom inside the fixture and limiting the movement of the pin. After the pins are secured in the locking plate, the upper PCB is inserted and locked in place to prevent shifting during soldering of the through-hole joints. Each through-hole is manually soldered using solder wire. In the third step, SAC305 solder paste is printed on the bottom board using a 5 mil thick stencil onto the copper pads. To create a sufficient gap for the solder paste to reflow in between the pad and the pin flange, 5 mil thick precision washers were placed along with the standoff spacers. The final gap between the pin and the pad was roughly two mils larger than the stenciled solder paste height. The larger gap accommodated space for the pins to descend down onto the solder paste during oven reflow since the through-hole solder joints undergo a secondary reflow process.

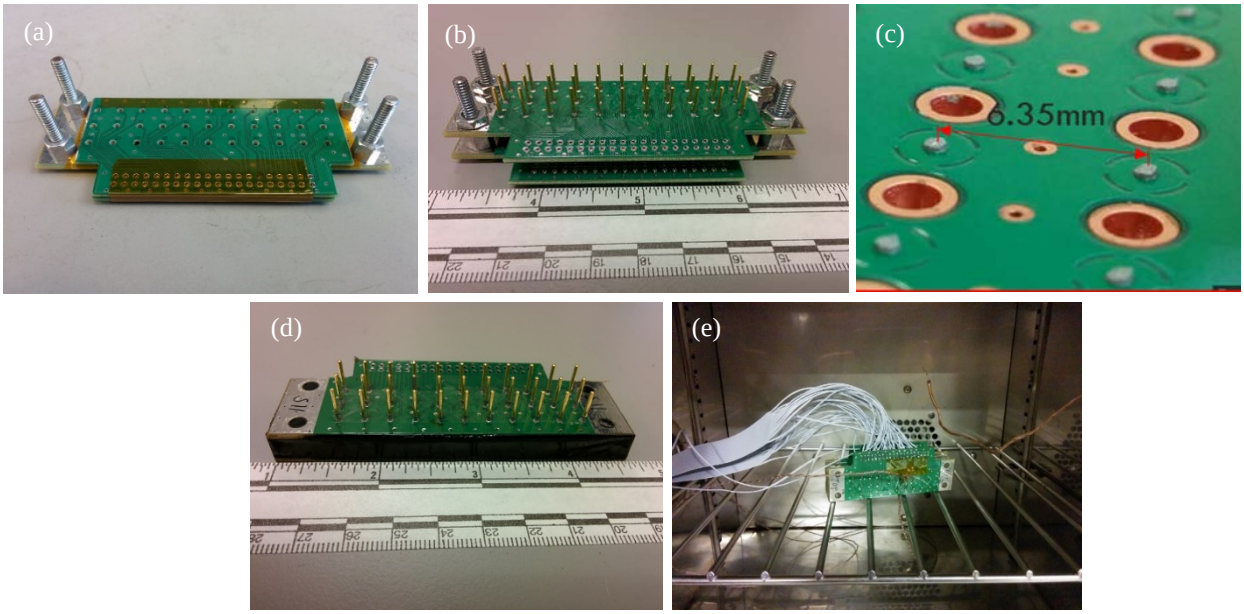

Figure 3 Specimen assembly steps: (a) alignment of locking plate (b) through-hole soldering (c) stencil surface mount solder (d) potted specimen with 6mm standoff height (e) wire connections.

After the reflow operation, the specimen is inspected using x-ray imaging to detect excessive voiding and wetting issues. Post inspection, polyimide tape is wrapped around three sides of the specimen to cradle the potting material during cure. Each of the selected potting materials is cured at the lowest recommended temperature to prevent accumulation of residual creep strain in the solder and avoid exothermic temperature during epoxy cure. Three standoff heights are initially selected: 4mm, 6mm and 12mm. The standoff height allows control of the potting height which in turn prescribes the displacement range during thermal expansion of the potting and impose displacement controlled loading conditions on both the through-hole and the surface mount joints. Reflowed surface mount solder pads have an average height of 120µm and a diameter of 1.5mm matching the contact area of the brass flange. Height of solder pads varied ±40µm from the average recorded value. Use of the PCB allowed for resistance measurements of each pin during thermal cycling and capture the number of cycles to failure for 33 individual solder joints in each specimen.

Selecting the temperature range controls the stress-strain state of solder joints during thermal cycling. Adjusting the mean cyclic temperature to above or below room temperature imposes a tensile or compressive mean strain, respectively. Specimens with potting material PM1 are tested under a temperature range of 100ºC with 12 mm standoff height resulting in accelerated failures resembling an overstress failure. Cross-sections of the specimen shown in Figure 4 revealed failure of the

copper layers in the though-hole copper barrels along with cracks in the solder surface mount pad. Extensive cracking in the epoxy is observed at the center of the specimen and large separation of the epoxy from the solder joint and brass pins are observed.

Figure 4 Specimen cycled at 25-125ºC thermal cycling showing epoxy separation and cracking around pin flange and ripped copper barrels in through-hole solder joints.

The thermal cycle selected crossed the T_g of PM1 resulting in strains large enough to separate the copper plating from the FR4 laminate material. The standoff height of the specimen was then reduced to 6 mm and 4 mm to prevent cracking of the epoxy by reducing strain range on solder joints. Similar failure of the copper barrel was observed but with prolonged cycles to failure. During thermal cycling with negative mean cyclic temperature, failure of the solder joints resulted from pad cratering. Through-hole joints did not show any damage accumulation; however, large percentage of the solder pads failed almost simultaneously due to large bending of the specimen during the compressive stresses potting material generated in Figure 5. No cracks were evident in the solder pad during compressive mean strain cyclic loading.

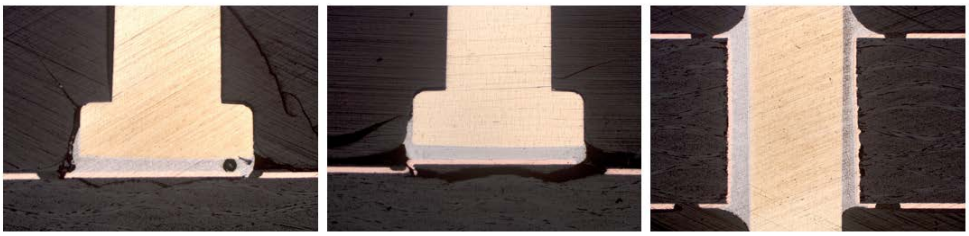

Figure 5 Specimen cycled at 45ºC to -50ºC thermal cycling showing cracking in the epoxy surrounding pins. Pad cratering in surface mount joints. Undamaged through-hole solder joints.

After thermal cycling with various potting materials and observation of failure mode by cross-sections, it is determined that the through-hole joints almost always facilitate more damage than surface mount joints and do not allow to track damage in the solder pads using resistance measurements. To confine the axial loading to the surface mount solder, a through-hole solder joint should not be used with a large volume of epoxy potting material in thermal cycling which crosses the material's T_g.

Thermal Cycling Profiles

To provide a fundamental understanding of the stress state in the solder joints a simple compatibility displacement equation is used. Equation1gives a representation of the force in the solder joint due to coefficient of thermal expansion mismatch and elastic modulus of the solder and the potting material. This relationship assumes a purely linear elastic interaction between the solder and potting expansion and serves as preliminary criteria for matching potting material with a thermal profile.

$$F = \frac{\Delta T(\alpha_2}{\frac{1}{A_1 E_1} +} \qquad (1)$$

Three thermal cycles were selected for this study and are shown in Figure 6. The thermal cycles represent the recorded temperature at the center of the specimen. Due to the large volume of potting materials, the large thermal mass of the specimen slows down the temperature transfer from the chamber air to solder joints. All three temperature profiles used an average of 10-minute dwell time and a ramp rate of 15 ºC/minute.

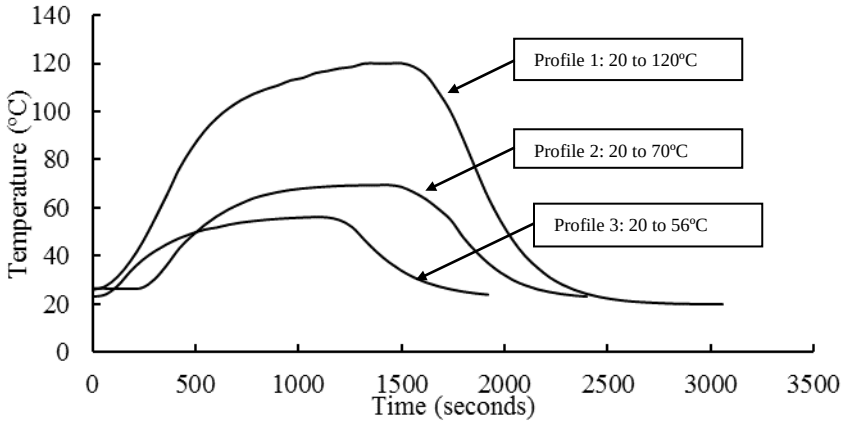

Figure 6 Thermal cycle profiles used with selected potting materials

With the low temperature range of profile 3, the cyclic rate was approximately 2 cycles per hours which is known to be more damaging to solder under thermal cycling range of -40 to 125ºC [9]. It is known that longer dwell time causes more creep in solder joints. Fatigue life of lead-free solder decreases significantly with an increase of dwell time from 15 to 30 minutes and beyond for thermal profiles with a peak temperature of 125ºC [10]. Therefore, consistent dwell times in both low and high temperature dwell periods were maintained.

Modified Specimen Design

The second iteration of the specimen uses a similar board layout with solder mask defined pads to mitigate pad cratering. The through-holes are enlarged to fit the larger swage pins and surface mount pads opening is adjusted to match the pin diameter of 760 µm. Length and width dimensions of the redesigned boards are kept unchanged as well as the pin count. Several changes are made in order to accommodate the swage pin and strengthen the solder pad. Through-hole traces are routed to the 2nd and 3rd layers respectively. Modified specimen configuration with the new swage pin connections is shown in Figure 7.

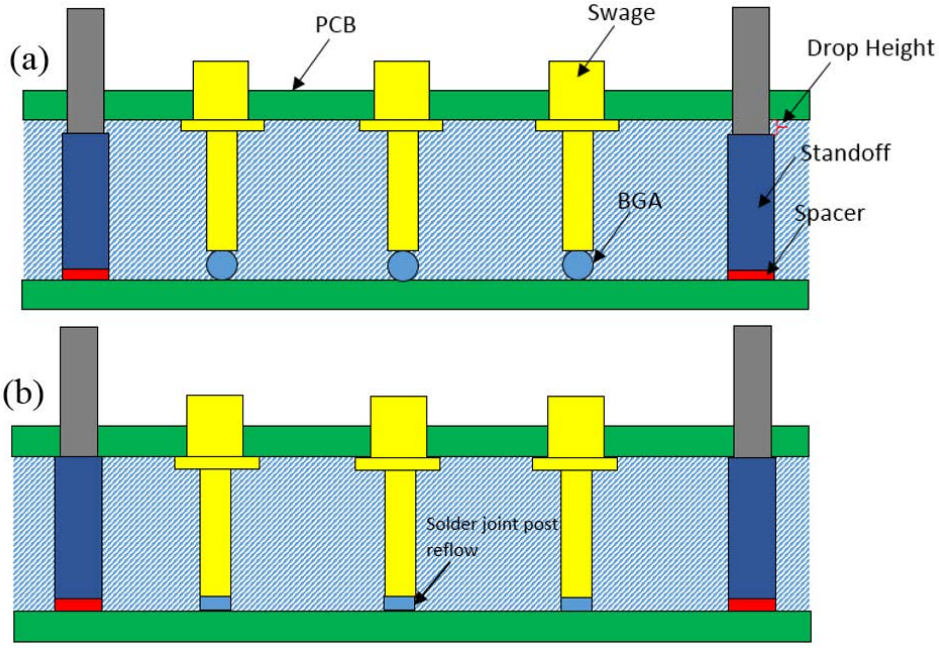

Figure 7 Illustration of specimen redesigned configuration (a) before reflow (b) post reflow.

Choosing a swage to replace the through-hole solder joints provides a stronger contact with the upper board but eliminates the adjustability of controlling the standoff height and changing the potting material volume. Therefore, this design decision limits the number of parameters in charge of changing the stress and strain on surface mount solder joints compared to the previous specimen design. Due to the smaller aperture of the new swage pins, two solder joint types were used: solder paste

and solder sphere. Figure 7 shows specimen assembly steps for the modified specimen. An aluminum fixture was machined to support the new pins for swaging. After swaging procedure, solder spheres are placed and aligned on copper pads using tacky flux. Thin shim spacers are used to adjust the drop height during reflow and control the final height of the solder joint. Drop height is adjusted based on the desired height of the solder joints. 760 µm diameter SAC305 solder spheres are used along with 14 mil spacers at each corner to achieve an average final solder height of 500 µm.

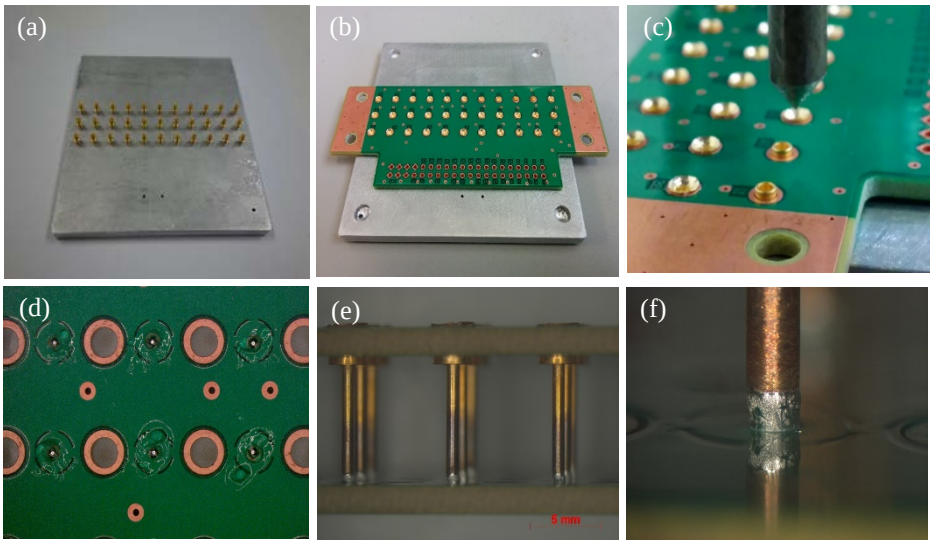

Figure 8 Modified specimen assembly process (a) pin swage fixture (b) board alignment with pins (c) swage procedure(d) solder balls placed in tacky flux (e) specimen post reflow (f) close up of as reflowed solder joint prior to potting.

Solder height can be adjusted by selecting solder spheres with smaller diameter and shim spacers. In these experiments a single solder sphere size is used to limit variables affecting stress level on solder joints. Initially, solder joints are made using SAC305 solder paste with 8 mil stencil with an aperture of 0.8 mm and similar pitch size to copper pad layout. Since larger volume of solder paste is used compared to the previous design, overprinting solder paste on copper pads compensated for volume shrinkage of solder paste during reflow. X-ray imaging post reflow is performed to inspect joint quality for voiding and alignment. Figure 9 shows x-ray images of solder joints with voids and misalignment with copper pad and brass pin. Misalignment of solder joint is caused due to tolerances in mounting and alignment of the swage board with the stenciled paste but did not exceed a concentric offset distance of 80 µm between the lower and upper faces of the solder joint.

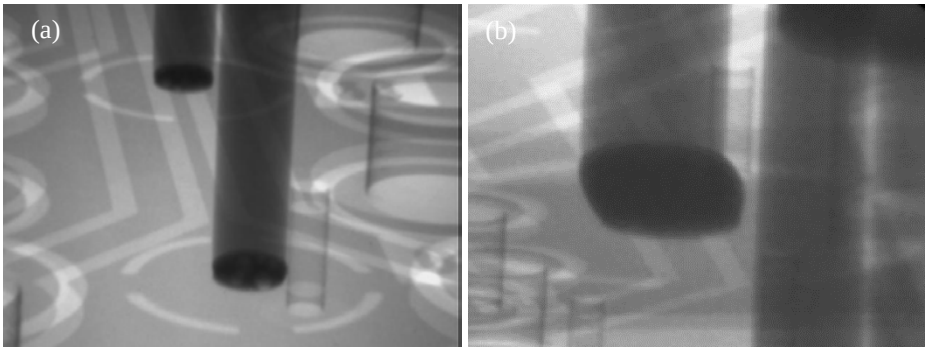

Figure 9 Oblique angle view x-ray of surface mount solder pads after reflow.

Specimens assembled with solder paste and various potting materials are cross-sectioned as shown in Figure 10. Fatigue crack growth through the bulk of the solder joint along with large void is evident. It is known that excessive voiding promotes bridging of fatigue cracks and potentially reduce the effective fatigue resistance of the solder. Misalignment of the solder joint is also shown and is of critical significant to axial loading. Since the solder joints are loaded in tension during thermal expansion, the stress state at the bulk solder depends on consistent cross-sectional area throughout the length of the joint. When skewed solder joints are loaded in tension, the stress state in the material transforms to a mixed tensile and shear loading. BGA joints exhibit multiaxial stress state due to the round features in their geometry. The goal of the reflowed solder joint was to reduce the shape convexity and simplify the stress state under axial loading.

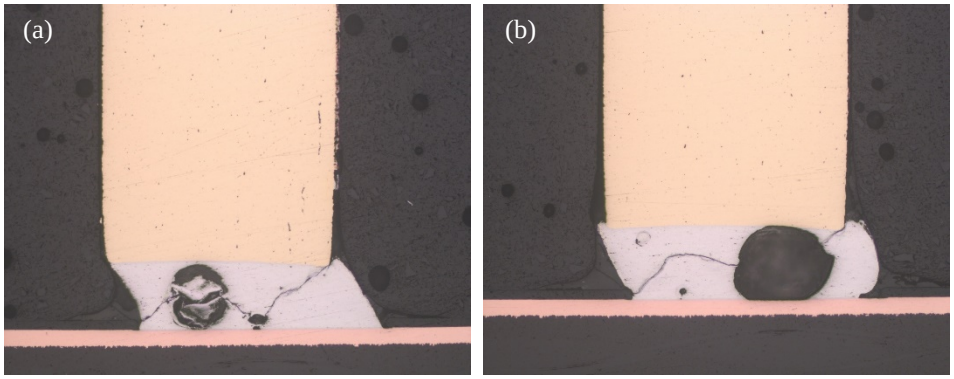

Figure 10 Solder joints made with SAC305 solder paste with excessive voiding and overstress cracks

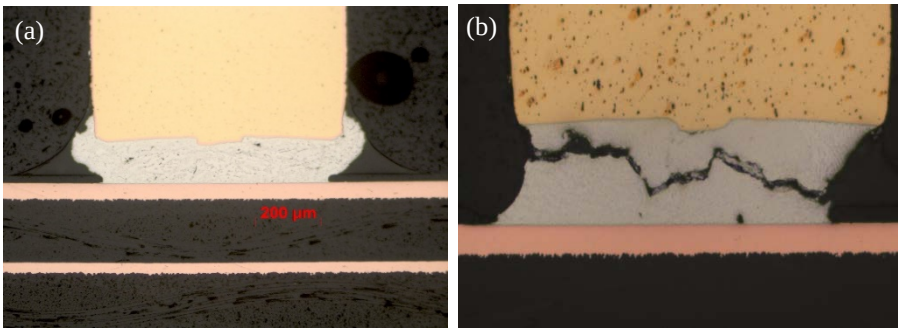

Figure 11 Improper solder joints created with 8 mil stencil (a) solder joint with wetting (b) hourglass shape joint.

In addition to skewed solder joints, another issue encountered with inconsistent solder joints during testing is shown in Figure 11. Joints in which wetting to the pin sides occurred were not able to capture the change in resistance since the crack would not fully propagate through the stress relaxed region and maintain consistent electrical contact preventing detection of electrical discontinuity. Another issue encountered with hourglass shaped solder joints which occurred due to larger standoff height and resulted in starving solder paste during reflow forming an hourglass shape. Specimens with hourglass shaped joints showed intermittent failure rates due to the different stress concentration caused by the hourglass shape. Solder spheres of SAC305 solder alloy eventually replaced solder joints made with solder paste due to the frequent inconsistencies of the specimen assembly and reflow procedures. From the compatibility displacement equation, PM6 was selected with temperature profile 3. At the selected temperature and CTE and E properties of PM1, failure of solder joints in the specimen varies from 1 to 232 thermal cycles. At the low temperatures of temperature profile 3, cyclic loading mostly resembles that of fatigue loading under isothermal conditions due to the low peak temperature.

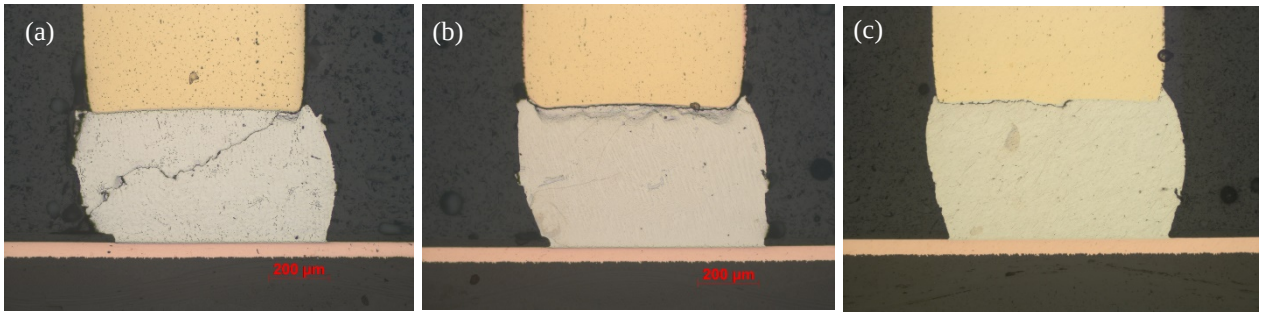

Figure 12 Cross-sections of specimen potted with PM6 cycled with profile 3 showing (a) 45º crack though bulk solder (b) crack at intermetallic interface (c) partially cracked joint

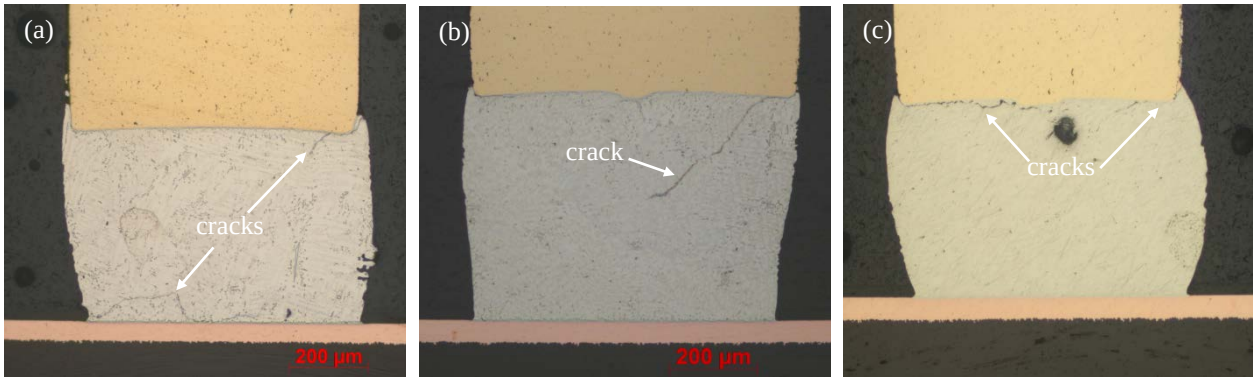

Figure 13 Cross-sections of specimen potted with PM6 cycled with profile 3 showing (a) 45º crack though bulk solder (b) crack at intermetallic interface (c) partially cracked joint

After cross-sectioning the specimen, a slight variation in solder joint height was evident from the specimen corner near the standoff spacers to the center of the specimen. Solder joints closer to the standoff spacers were found to have a slightly shorter height than the joints at the center. A reason for this variation was found to be the curvature of the PCB itself which contributed to the variation in joint height. It is known that shorter joints will experience larger stresses and strains due to the relative difference between solder joint and potting material height. This difference in solder joint height and specimen configuration also helped influence the fracture mode. Figures 12 and 13 show solder joints at various locations in the specimen post thermal cycling. Cross-sections of various solder joints on the same row of specimen tested with potting material PM6 with temperature profile 3 are compared. Solder joints from the specimen corner exhibit a 45º crack growth through the bulk of the solder while joints from the center exhibit cracking in the solder matrix around the intermetallic layer. One reason for variation in cycles to failure was due to variability in solder joint height. Solder balls height in BGA packages is one of the most important parameters affecting reliability. With taller solder joints fatigue life can be drastically increased due to a lower strain range the joint experiences compared to a shorter solder joints [11].A difference in the solder joint height could also influence the distribution of stresses and strains and be more prone to fail under certain orientations. More testing is necessary to correlate certain test conditions to the failure type observed in solder joints.

Finite Element Modeling

To model the stress in the solder joint, specimen geometry is constructed in production FEA software. Finite element (FE) simulation of the specimen was performed on the full specimen geometry and meshed using three-dimensional hexahedral elements (Continuum, 3-D, 8-node, Reduced integration). This element type has been proven to accurately model visco-plastic behavior of solder [12]. Schubert's constitutive model shown in equation (2) is used to simulate creep behavior of SAC305 solder [13].

$$\varepsilon^{cr} = A_1(sinh\alpha\sigma)^n \exp\left(-\frac{H_1}{kT}\right) \qquad (2)$$

Model parameters used in the constitutive equation are displayed in Table 2. Brass pins are modeled as thermo-elastic material with temperature dependent E. All potting material properties are assumed to be perfectly elastic neglecting any viscoelastic effect except for PM1 which included temperature dependent CTE and E properties as shown in Figure 1. Each simulation initiated at room temperature with the assumption of zero stress state to be 20 ºC ignoring any possible residual stresses introduced during reflow or cure of potting materials. The intermetallic layer was not included in the analysis since it has been shown to have only a slight effect on fatigue life evaluation of lead-free solder [14].

Table 2: Coefficients for constitutive relationship

A_1	α	n	H_1	k
277984	0.02447	6.41	54041	8.314

Table 3: Material Properties used in FEA Model

Materials	PCB	Copper	Brass	SAC305
E (MPa)	33986	118590	110000	5000
ν	0.13	0.326	0.35	0.3
CTE (ppm/°c)	$16.9x10^{-6}$	$16.7x10^{-6}$	$17.6x10^{-6}$	$20x10^{-6}$

Material properties used in modeling are shown in Table 3. Potting material properties for PM2 through PM6 are assumed to have constant CTE and E throughout the temperature profiles. Figure 14 shows the specimen and solder joint geometry constructed in the production FEA software. Quarter symmetry is not implemented due to asymmetric potting geometry layout around brass pins. Solder joint geometry was kept identical throughout the specimen to simplify the analysis. 100 µm separation between pin, solder and potting was used to prevent over constraining specimen expansion and generating hydrostatic stress on the solder due to the large volume of potting materials. Local geometry was used with coarse and fine mesh solder joints as shown in Figure 14. An initial run with coarse models was made for each potting material properties at different temperature profiles to determine the critical joint location. Fine mesh local geometry was then substituted in the critical joint location.

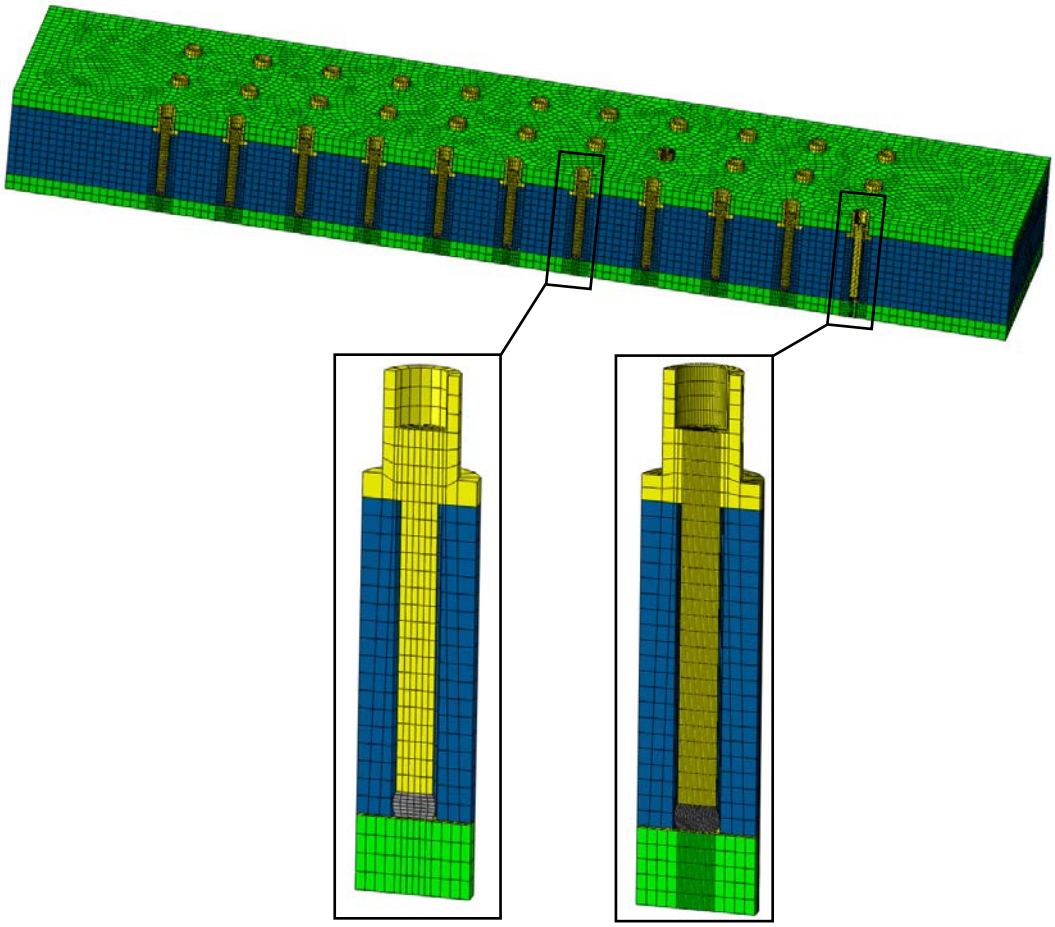

Figure 14: Section view of specimen model showing coarse and fine mesh local geometries

Axial stress and strain in solder joints were averaged over 25 µm thick layer of elements at a sufficiently large distance from the solder/brass interface to avoid potential edge effects. Temperature dependent CTE and E of potting material PM1 are applied to the compatibility of displacement equation to give a measure of axial stresses solder experiences during potting expansion as it is thermally cycled across its T_g. Figure 15 shows the axial stress in the solder as a function of temperature from DMA and TMA data. The initial stress increase prior to the T_g is maintained linearly similar to the behavior of thermally stable materials. The stress level reaches a maximum value which is governed by the shift in material properties around the T_g more so then the specimen geometry. Drop in stress occurs only after the modulus decreases sufficiently to

accommodate thermal expansion of the potting material. The relative rate of modulus decrease compared to the rate of CTE increase allows a temporary intensification of axial stresses over a narrow window of temperature range. This temporary peak in stress could be sufficiently large to contribute to the reduced fatigue life observed in flip-chips with underfill. The axial stress generated in the solder using this elementary analysis is useful in explanation of the failures observed in the through-hole solder joints of the original specimen design as it was thermally cycled across the T_g. Potting materials with a larger difference in their CTE across the T_g could generate even higher stress levels. It is possible to mitigate axial stresses in such a manner as to select materials with a specific combination of T_g, CTE and E for a desired operating temperature [15-16].

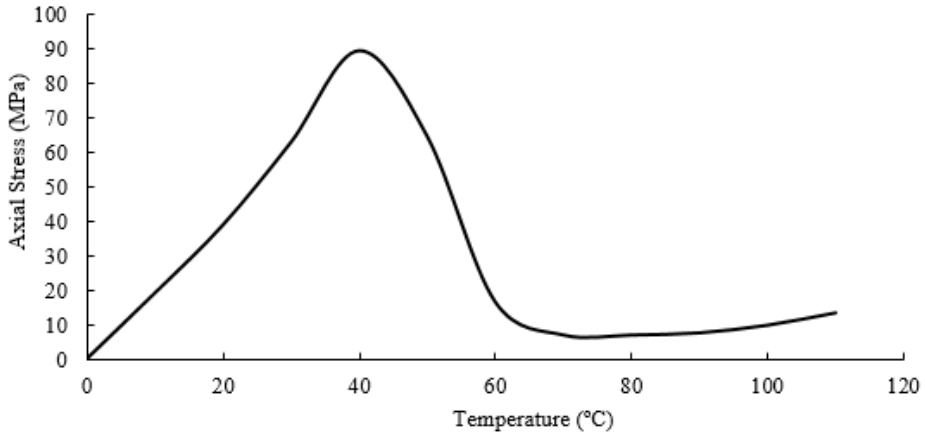

Figure 15 Axial stress with temperature in solder using temperature dependent CTE and E of PM1

Comparison of stress and strain behavior throughout the various joints in the specimen is performed to show the effect of potting material properties. Figure 16 shows the von Mises stress plot for two solder joints in the specimen with PM2 properties under temperature profile 2. Noticeable differences in the magnitude of stress distribution can be seen from the center and corner joints. Highest stress is observed at the interface of the solder joint with the brass pin surface and at the center of the solder joint. During thermal cycling, the stress state in the solder shifts from tensile to compressive. It is generally assumed that solder joints do not experience damage under compressive loads during cold dwell periods of thermal cycles.

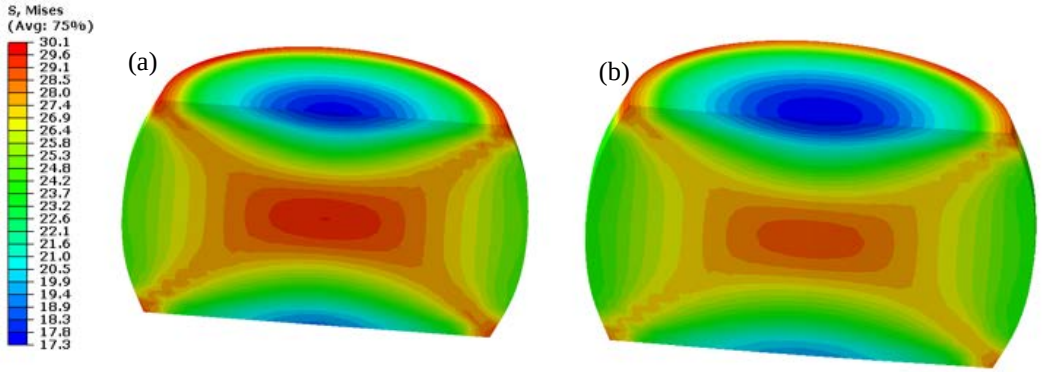

Figure 16 Von Mises stress plot in (a) center (b) corner joint for specimen with PM2 potting at the end of high temperature dwell of the 1st cycle

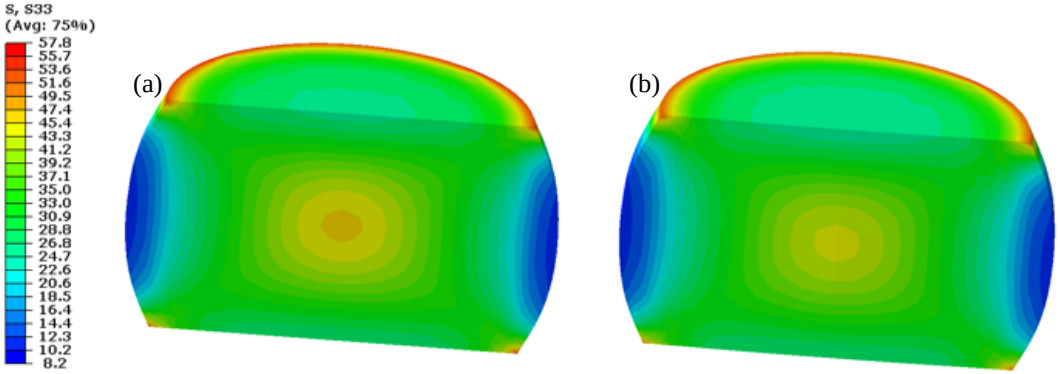

Figure 17 Axial stress plot in (a) center (b) corner joint for specimen with PM2 potting at the end of high temperature dwell of the 1st cycle

The FE model correlates well in identifying the area with largest stress in which crack initiation and propagation under tensile loading is found to occur. Von Mises stress plot shows large stresses bridging from the corner to the center of the solder joint under axial loading which could explain the 45º crack initiation and growth in corner joints. A possible explanation to the variation in crack path could be attributed to the combination of shear and tensile stresses throughout solder joints with different heights in the specimen. Qin et al. showed that with decreased solder joint height, the concentration of strain energy at the interface of solder and pad decreases and the fracture location of the solder joint changes from the intermetallic interface to the middle of the solder matrix [17]. The fracture location of solder joints under tension with low and high standoff heights follows that of shear loading with cracking originating at the middle of solder and solder/IMC interface, respectively. This phenomenon support the contribution of a lower solder joint height on influencing the crack path than the slight variation in stress. Figure 17 represents the axial stresses in the solder joint which are significantly higher than the von Mises stress. This demonstrates the loading mode solder joints are placed under during thermal cycling. Largest tensile and compressive loads are found at the corner of solder joints at the upper and lower interfaces with the brass pin and copper pads respectively. As the dwell alternates from high to low temperature the local stress in the interface changes from tensile to compressive along with the stress state at the bulk of the solder which is shown to be relatively uniform in the bulk of the solder.

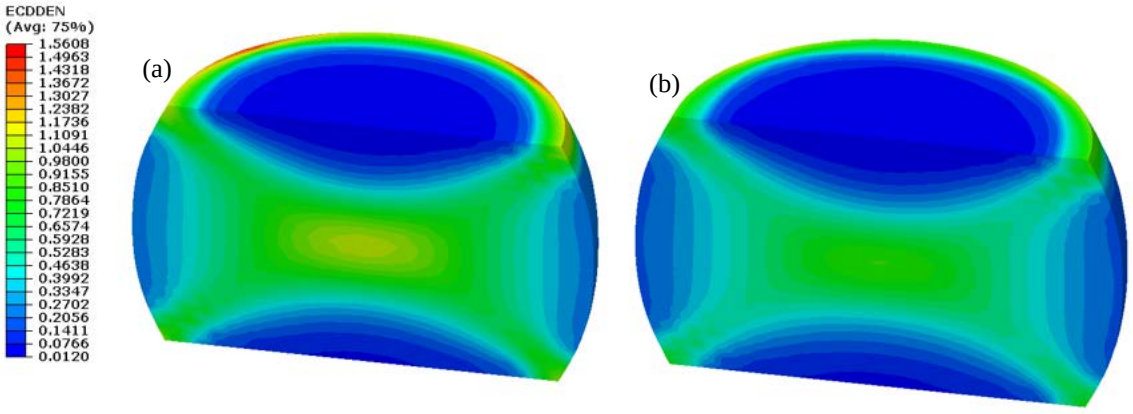

Figure 18 Accumulated creep strain energy density plot of(a) center and (b) corner joint for specimen with PM6 under temperature profile 3 for the 3rd cycle.

To give a perspective on the variation in fatigue life of the solder joint in the specimen, accumulated strain energy density plot is shown in Figure 18 for the center and corner joints in specimen with potting material PM6 under temperature profile 3. The area with highest accumulation of energy matches that seen in the von Mises stress plot. Higher accumulated creep strain energy density is found in solder joints located at the center row of the specimen with lower energy in corner joints and joints located around the perimeter of the specimen. Solder joints at the corners are subjected to slightly lower axial stress and strain but experience larger shear stresses. The difference in magnitude of shear stress and strain is not considered in this analysis due to the low magnitude observed in FE modeling.

The effect of potting material on the strain state of the solder is shown in Figure 19. Four potting materials with different CTE and E are compared for the same temperature profile. It can be seen that the material with highest mean tensile strain

amplitude is PM4 with a CTE and modulus of 87 ppm/ºC and 340 MPa respectively. The combination of low modulus and high CTE proves to generate higher strains. Since the potting material expansion is controlled by the temperature profile, the resulting deformation the solder joints experience are under displacement controlled loading. The corresponding stress behavior of four potting materials in shown in Figure 20. Since the potting expansion is constrained between the two PCB boards, the resulting maximum stress solder joint experience occurs prior to the maximum strain which follows the peak temperature. This behavior allows for stress relaxation to occur while creep strain is accumulating during dwell times. The accumulation of the creep strain is also influenced by the thermal mass of the potting material used. With larger thermal mass, the slow thermal transition from ramp rate to dwell period reduces the accumulation of creep strain and allows for longer stress relaxation.

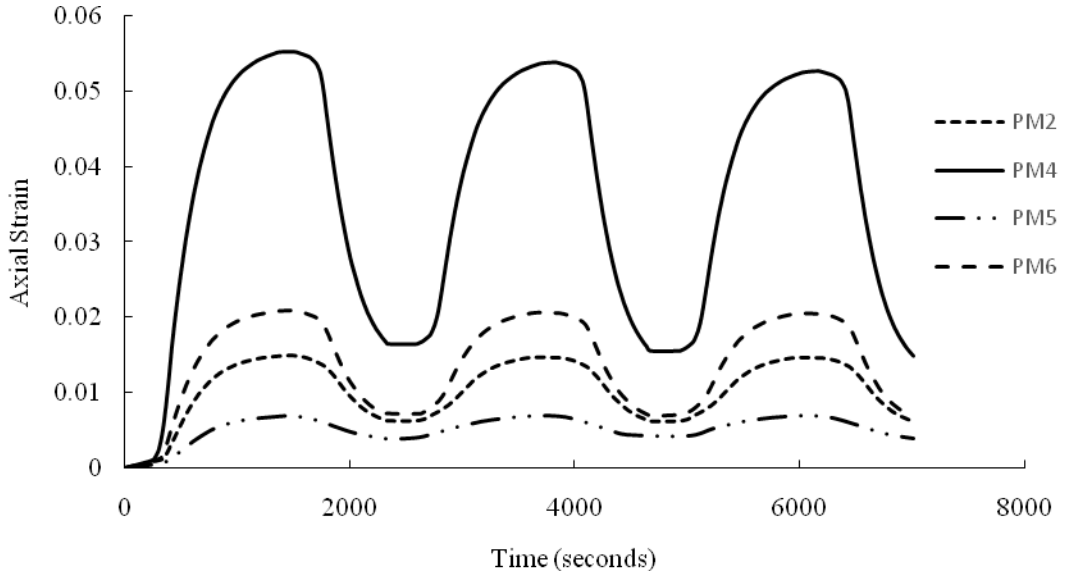

Figure 19 Average axial strain with time for several potting materials under temperature profile 2

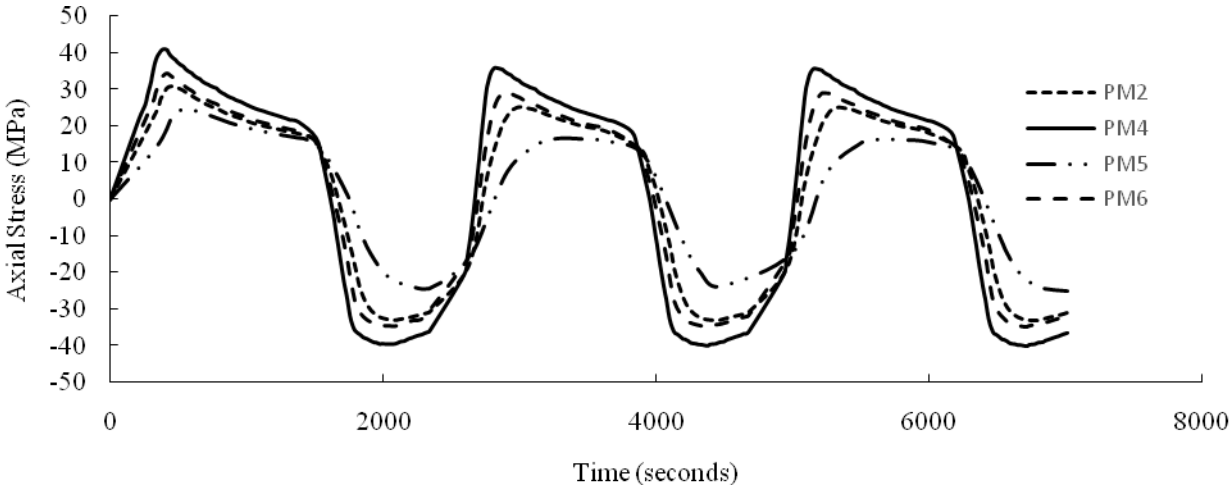

Figure 20 Average axial stress with time for several potting materials under temperature profile 2

Selection of the correct temperature profile with each potting material is proved to be a critical factor in achieving a desired strain level for cyclic loading. When potting material is paired with a specific temperature range the strain level will reach a comparable magnitude that reduces or increases time to failure. At low temperatures, the strain level imposed on the solder could be low enough to transition the loading conditions from low to high cycle fatigue and high strain levels will result in an overstress failure. Attaining low cycle fatigue conditions greatly depends on combination of the CTE, E and temperature range. Figure 21 shows axial strain with time for PM4 under the three tested temperature profiles. Even with potting material with low modulus, solder joints are subjected to very large tensile strains. With an increase in peak temperature a comparable increase in mean strain level is observed. The peak strain level observed for temperature profile 2 and 3 correlate to the overstress failure observed in specimens. Overstress failure of the solder joints occurs at the first thermal cycle for specimen tested with PM4 under temperature profiles 2 and 3. Low cycle fatigue was achieved for the same specimen and potting material configuration under temperature profile 3. The mean strain level reached with temperature profile 3 corresponds to isothermal low cycle fatigue results under shear loading in previous studies.

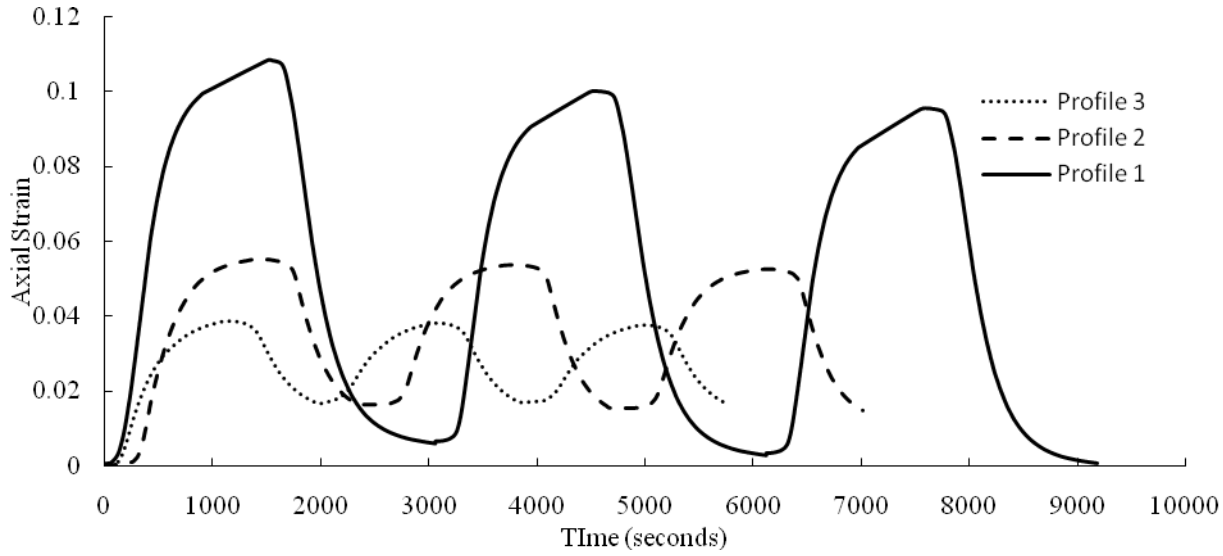

Figure 21 Average axial strain with time for PM4 under three temperature profiles

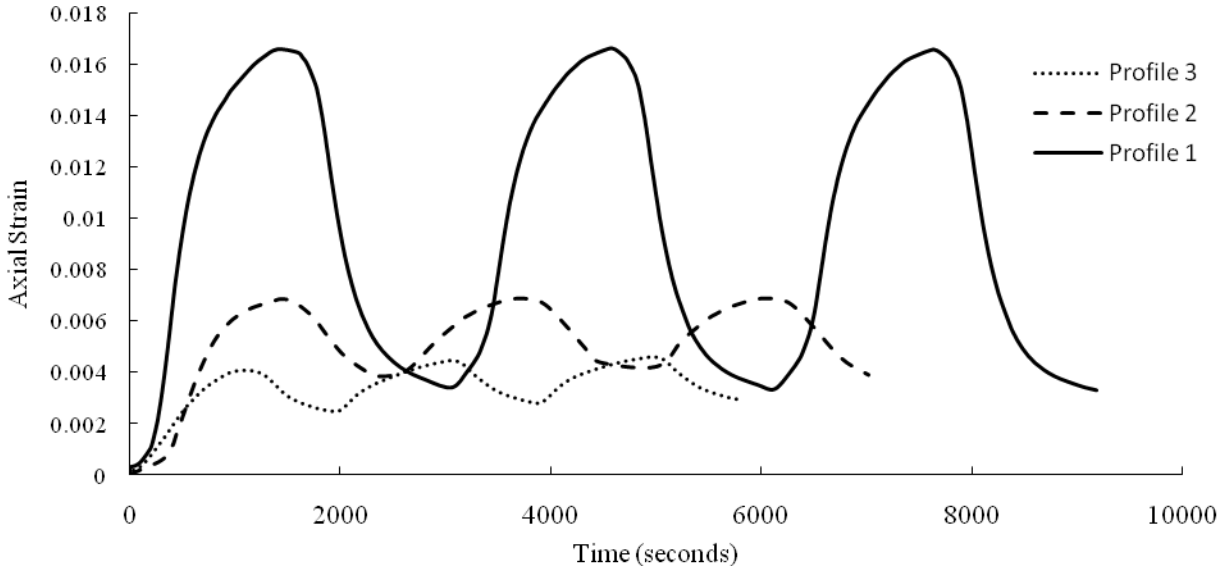

Figure 22 Average axial strain with time for PM5 under three temperature profiles

Figure 22 shows axial strain with time for PM5 under the three tested temperature profiles. The CTE and E of PM5 was 28 ppm/ºC and 10.7 GPa respectively. Potting materials with very low CTE values and high E are necessary to subject solder joints to similar strain level as materials with higher CTE and lower E. The strain level of PM5 with profile 1 is significantly lower than the strain level reached by PM4 with profile 3. Tests with temperature profiles 2 and 3 of PM5 were tested past 2000 thermal cycles with no recorded failures or observed crack initiation. The low axial strain level obtained using FE modeling in specimen with PM5 matches experimental results in which low cycle fatigue failures were not observed.

Variation in solder joint geometry should be incorporated into FE modeling to better represent the difference in stress and strain in each solder joint in the specimen. FE modeling used in this research is necessary for selecting the desired axial strains to be achieved during thermal cycling. An equivalent strain approach can be used to correlate the strain level between cyclic shear and axial test configurations for a better comparison of isothermal and TMF life testing under shear and tension-compression loading. Testing with temperature range from negative to positive temperatures will be performed to study fatigue life of solder joints with various mean strain conditions. Thermal cycling experiments of the specimen are currently being conducted to determine fatigue life under axial loading conditions at various temperatures.

Conclusion

The cyclic fatigue life of encapsulated solder joints is reduced significantly due to specific combinations of mechanical properties. The CTE and modulus of the encapsulant generates axial stresses and strain during thermal expansion. Understanding the fatigue performance of solder joints under predominantly axial loading is necessary for incorporating the contribution of axial loads to TMF life models. Therefore; a novel test coupon was constructed in order to subject solder joints under axial cyclic loading driven by thermal expansion of potting materials. The specimen has shown to induce axial tensile and compressive loads in BGA solder joints during thermal cycling. The test coupon enables simplified control of fatigue strain range with temperature by selection of encapsulant with desired material properties. Displacement compatibility equation with temperature dependent modulus and CTE properties are shown to associate the tensile stress level that represents a transition of failure mode from low cycle fatigue to overstress failure. However; the analytical equation fails to correlate to low cycle fatigue life regimes due to the displacement control nature of the specimen. Finite element analysis was performed to capture stresses and strains observed by solder joints in the specimen during thermal cycles. Fatigue cracks were found to propagate diagonally at 45-degree angle to the applied axial loading with a few exceptions in which fatigue cracks propagated parallel to the solder and brass pin interface. Potting materials with high CTE and low modulus were found to cause higher axial strains in solder joints compared to potting materials with low CTE and high modulus. Results from the test coupon could provide insight to the contribution of axial loading to fatigue life of solder joints and combined with shear based fatigue models to better predict reliability of solder interconnects in a variety of electronic packages under axial and mixed mode stress state.

References

[1] Kwak, Jae B., et al. "Deformation and strain measurement of flip-chip solder bump under in-situ thermal loading." *ASME 2009 International Mechanical Engineering Congress and Exposition*. American Society of Mechanical Engineers, 2009.

[2] Ghaffarian, Reza. *BOK─ Underfill Optimization for FPGA Package/Assembly*. Pasadena, CA: Jet Propulsion Laboratory, National Aeronautics and Space Administration, 2011.

[3] Liang, Ting, et al. "Torsional fatigue with axial constant stress for Sn–3Ag–0.5 Cu lead-free solder." *International Journal of Fatigue* 67 (2014): 203-211.

[4] Gao, Hong, and Xu Chen. "Effect of axial ratcheting deformation on torsional low cycle fatigue life of lead-free solder Sn–3.5 Ag." *International Journal of Fatigue* 31.2 (2009): 276-283.

[5] Andersson, Cristina, et al. "Comparison of isothermal mechanical fatigue properties of lead-free solder joints and bulk solders." *Materials Science and Engineering: A* 394.1 (2005): 20-27.

[6] Nadimpalli, Siva PV, and Jan K. Spelt. "R-curve behavior of Cu–Sn3. 0Ag0. 5Cu solder joints: effect of mode ratio and microstructure." *Materials Science and Engineering: A* 527.3 (2010): 724-734.

[7] Lee, Joon-Yeob, et al. "Study on the board level reliability test of package on package (PoP) with 2nd level underfill." *2007 Proceedings 57th Electronic Components and Technology Conference*. IEEE, 2007.

[8] Wilcoxon, Ross, Dave Hillman, Doug Pauls, and Dan White. "The Impact of Improper Conformal Coating Processes on BGA Solder Joint Integrity." SMTA International Conference Proceedings (2015): 870-882

[9] Chow, Seng Guan, et al. "Board level solder joint reliability modeling of embedded wafer level BGA (eWLB) packages under temperature cycling test conditions." *Electronics Packaging Technology Conference (EPTC), 2011 IEEE 13th*. IEEE, 2011.

[10] Fan, Xuejun, G. Rasier, and Vasu S. Vasudevan. "Effects of dwell time and ramp rate on lead-free solder joints in FCBGA packages." *Proceedings Electronic Components and Technology, 2005. ECTC'05.*. IEEE, 2005.

[11] Schubert, A., et al. "Thermo-mechanical reliability of flip chip structures used in DCA and CSP." *Advanced*

Packaging Materials, 1998. Proceedings. 1998 4th International Symposium on. IEEE, 1998.
[12] Fan, Xuejun, Min Pei, and Pardeep K. Bhatti. "Effect of finite element modeling techniques on solder joint fatigue life prediction of flip-chip BGA packages." *Electronic Components and Technology Conference, 2006. Proceedings.56th*. IEEE, 2006.
[13] Schubert, A., et al. "Fatigue life models for SnAgCu and SnPb solder joints evaluated by experiments and simulation." Electronic Components and Technology Conference, 2003. Proceedings. 53rd. IEEE, 2003.
[14] Chiou, Yung-Chuan, Yi-Ming Jen, and Shih-Hsiang Huang. "Finite element based fatigue life estimation of the solder joints with effect of intermetallic compound growth." Microelectronics Reliability 51.12 (2011): 2319-2329.
[15] Kornain, Z., et al. "Comparative study of different underfill material on flip chip ceramic ball grid array based on accelerated thermal cycling." *American Journal of Engineering and Applied Sciences* 3.1 (2010).
[16] Ong, Xuefen, Soon Wee Ho, Yue Ying Ong, Leong Ching Wai, Kripesh Vaidyanathan, Yeow Kheng Lim, David Yeo et al. "Underfill selection methodology for fine pitch Cu/low-k FCBGA packages." Microelectronics Reliability 49, no. 2 (2009): 150-162.
[17] Qin, H. B., et al. "Geometry effect on mechanical performance and fracture behavior of micro-scale ball grid array structure Cu/Sn–3.0 Ag–0.5 Cu/Cu solder joints." *Microelectronics Reliability* 55.8 (2015): 1214-1225.

Effect of Encapsulation Materials on Tensile Stress during Thermo-Mechanical Cycling of Pb-Free Solder Joints

Maxim Serebreni, Nathan Blattau, Gilad Sharon, Craig Hillman

DfR Solutions

Beltsville, MD

Presented at

IPC APEX EXPO 2017 Conference

San Diego, CA, February 14-16

Outline

- Background
- Development of new test coupon
- Test Coupon Construction
- Initial Failure Analysis
- Redesigned Coupon
- Experimental Results
- Modeling
- Conclusion and Future Work

Background

- Reduced fatigue life in BGA packages with underfill
- Axial strain and shear strain contribution to thermo-mechanical fatigue life
- How does axial loading contributes to reduction in fatigue life of BGA components

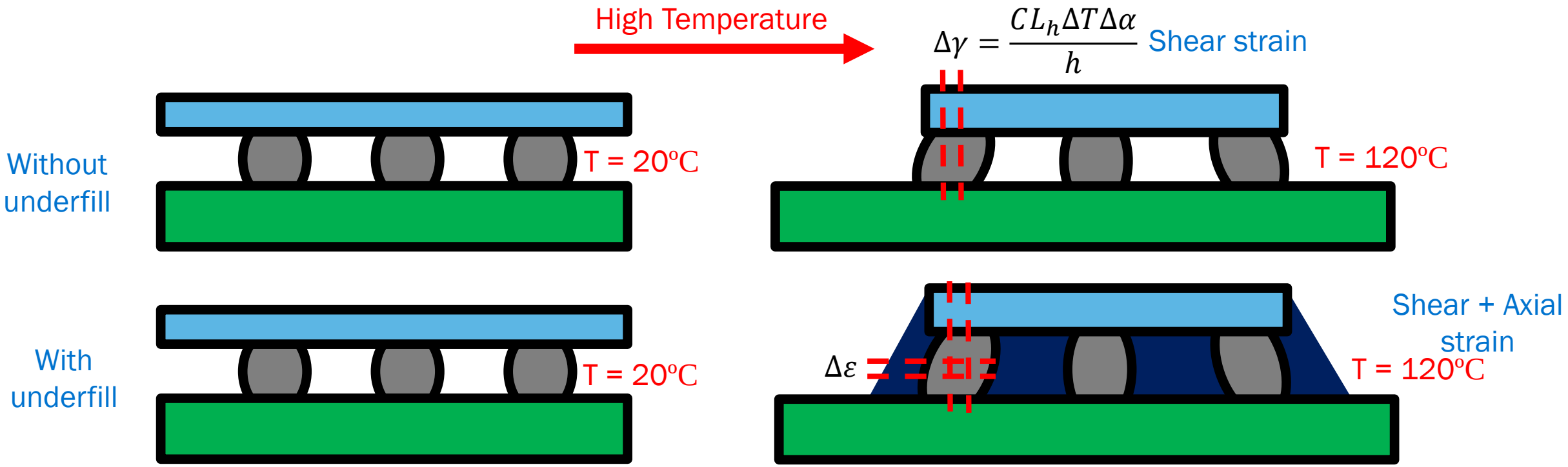

Background

- Isotropic expansion of underfill is constrained between the PCB and component causing axial strains in the normal direction to the board surface
- CSP package – 12x12, 228 I/O, 0.5mm pitch, SAC305 solder, 0.3mm ball diameter, 1 mm thick FR4 PCB.
- -40ºC to 125ºC, 10 min dwell, 15ºC/min ramp thermal cycles
- Full underfill shown to be more damaging than corner fill
- Both underfill show lower fatigue resistance than control

Underfill	Viscosity at 25°C (mPa.s)	Tg (°C)	CTE (ppm/°C)		Modulus (GPa)	Typical curing performance
			α1	α2		
A	375	69	52	188	3.080	8 minutes at 130°C
B	2000~4500	85	60	200	3.500	5 minutes at 120 °C

Sample	FCFU-A	FCFU-B	PCFU-A	PCFU-B	Control
α or $N_{63.2\%}$	3206	3640	3406	3932	4268
$N_{50\%}$	2844	3281	3100	3694	4059
$N_{1\%}$	712	988	1046	1796	2272
$N_{\text{First failure}}$	960	1046	1519	2251	2650
β	3.056	3.527	3.895	5.871	7.296
# Failures /# Samples	41/45	43/45	39/45	37/45	19/45

Shi, H. B., & Ueda, T. (2011, December)

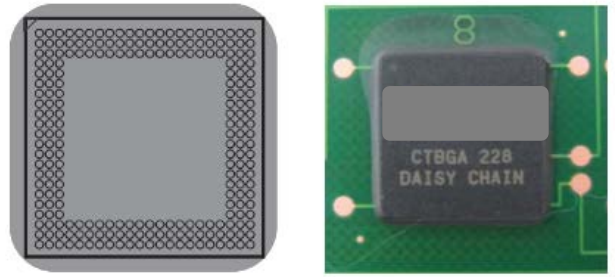

(a) Full underfill

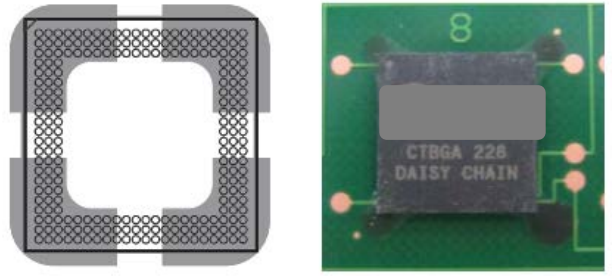

(b) Partial underfill

Development of New Test Coupon

- Developing a specimen to subject solder joints to cyclic thermomechanical fatigue under purely axial tension-compression loading. Control stress-strain behavior of solder joints with thermal cycle under predominantly axial loading.
- Ability to apply desired axial strain and temperature range by altering potting material and standoff height. Observe failure mode of solder joints under axial TMF.

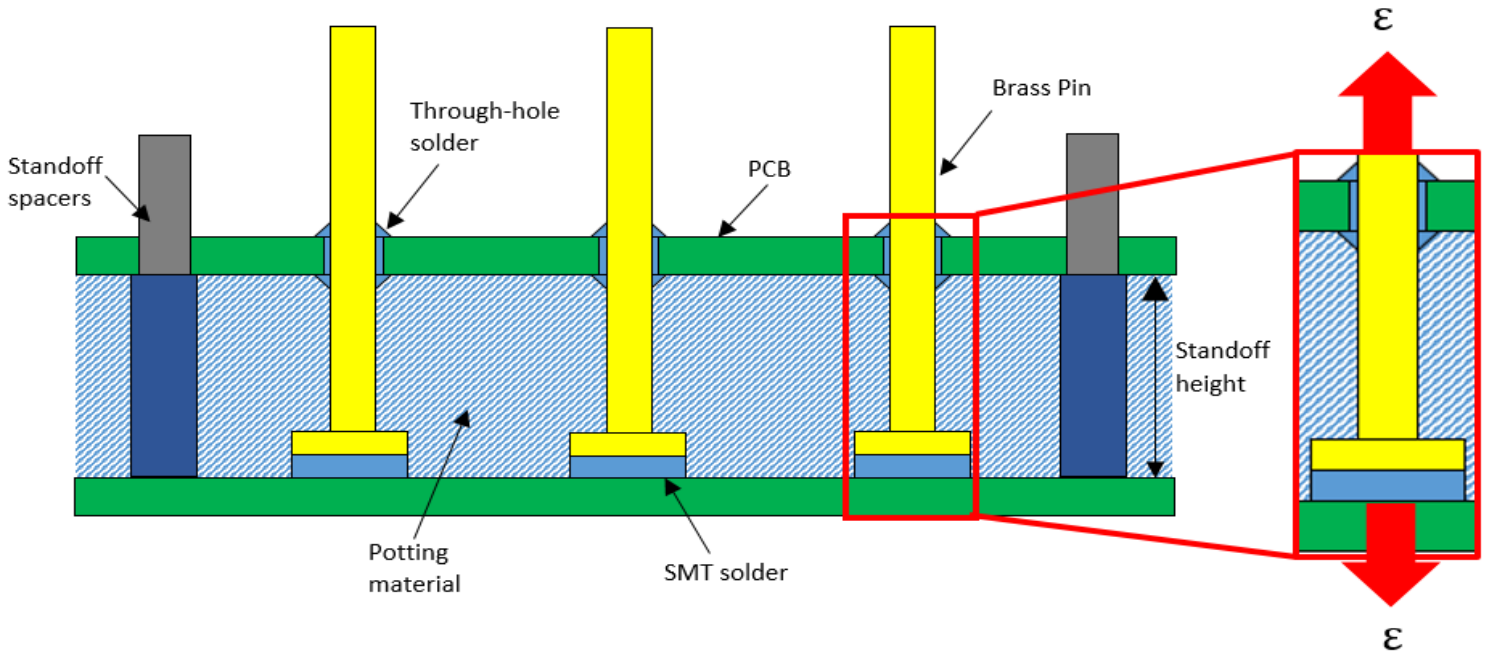

Test Specimen Construction

- Simplified construction procedure designed with minimal number of steps.
- Reduce sample to sample variation
- Easy scale up and reproduction
- Simultaneous testing of through-hole and surface mount solder joints

Pin flange retainer

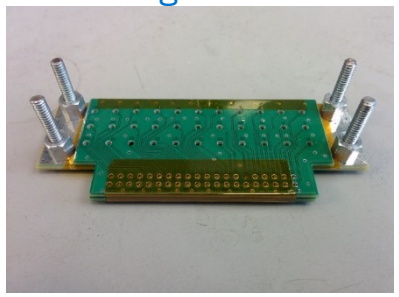

Insert pins

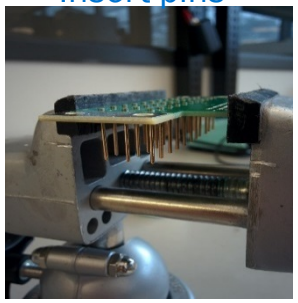

Solder through holes

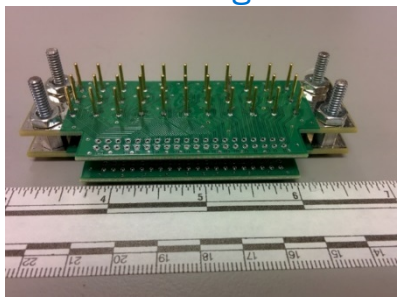

Stencil solder paste

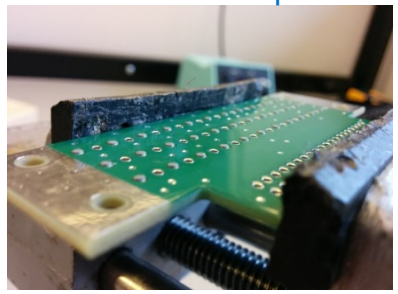

Reflow

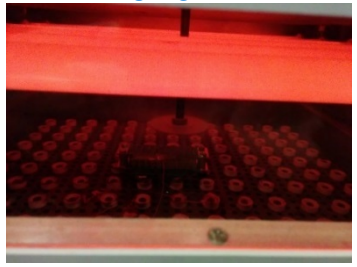

Specimen potting (12mm)

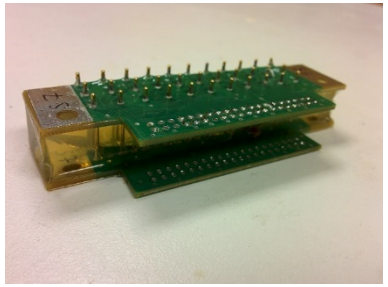

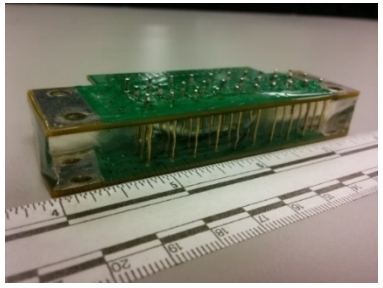

Thermal Cycling

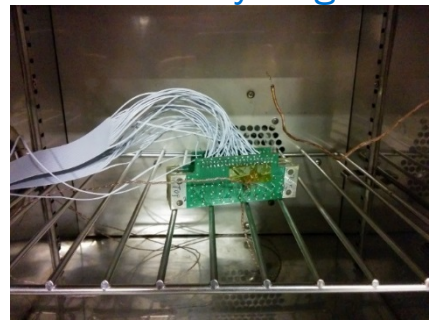

Initial Failure Analysis

- Thermal cycling 25C-125C showing large cracking in the epoxy surrounding pins. overstress failure of specimen. Pull apart TH joints.

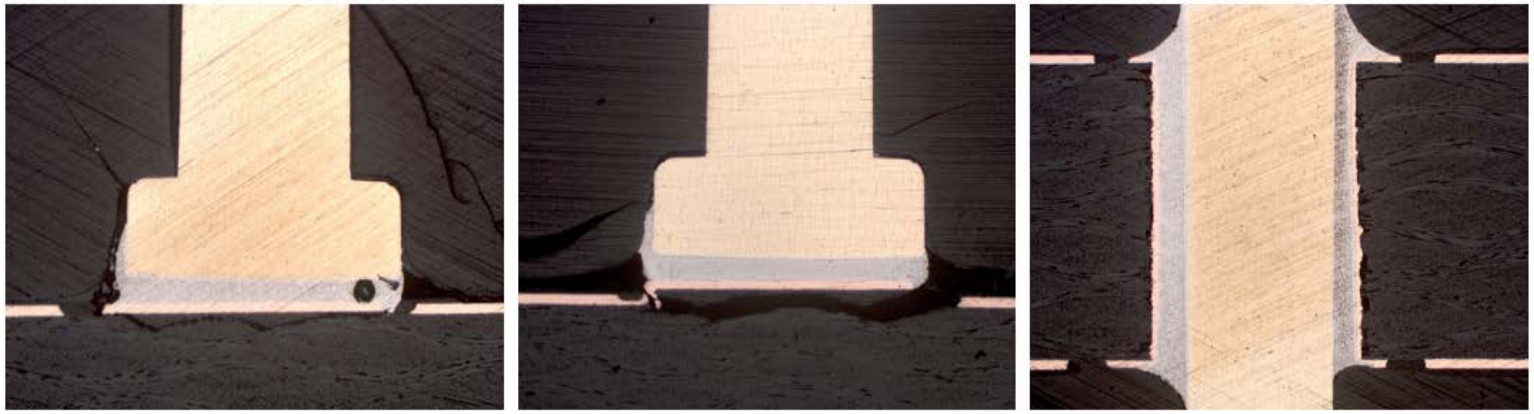

- Thermal cycling 45C to -50C showing large cracking in the epoxy surrounding pins. pad cratering failure mode. Through holes were not damaged

Initial Failure Analysis

- Transition of failure mode and location from high to low temperatures
- Failure location in the specimen is driven by potting materials temperature dependent properties

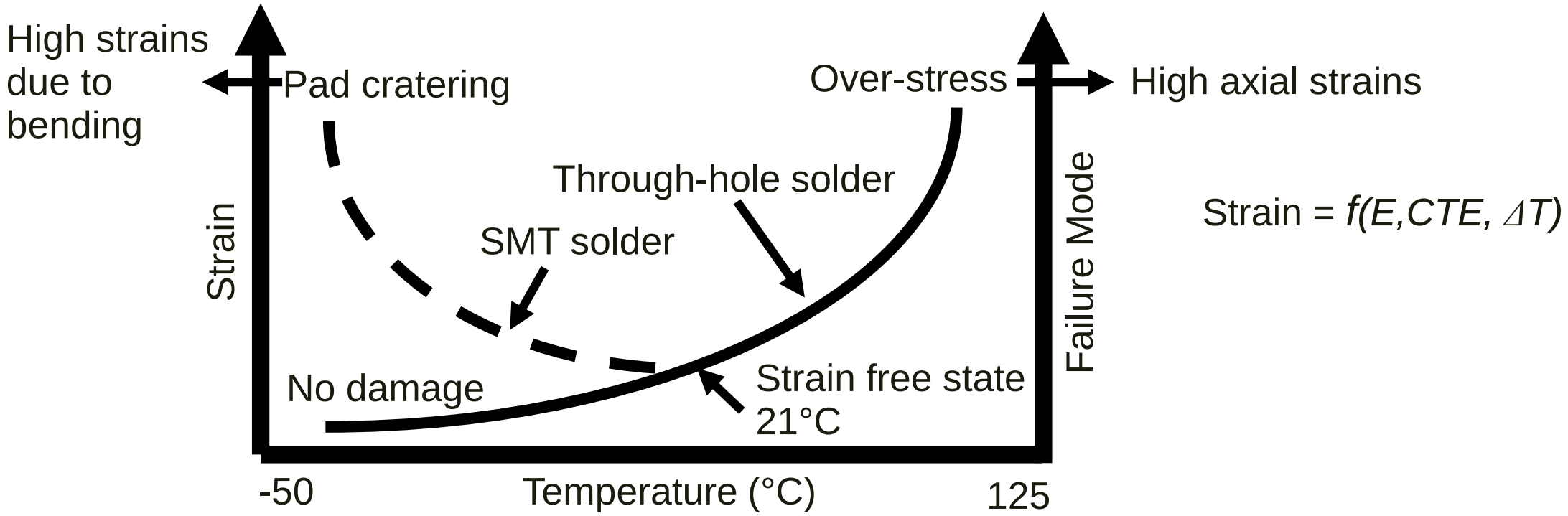

Strain = $f(E, CTE, \Delta T)$

Redesigned Coupon

- Eliminate potential through-hole failure.
- Fix potting volume height.
- Adjustable solder joint height using selection of BGA solder diameter and drop height.

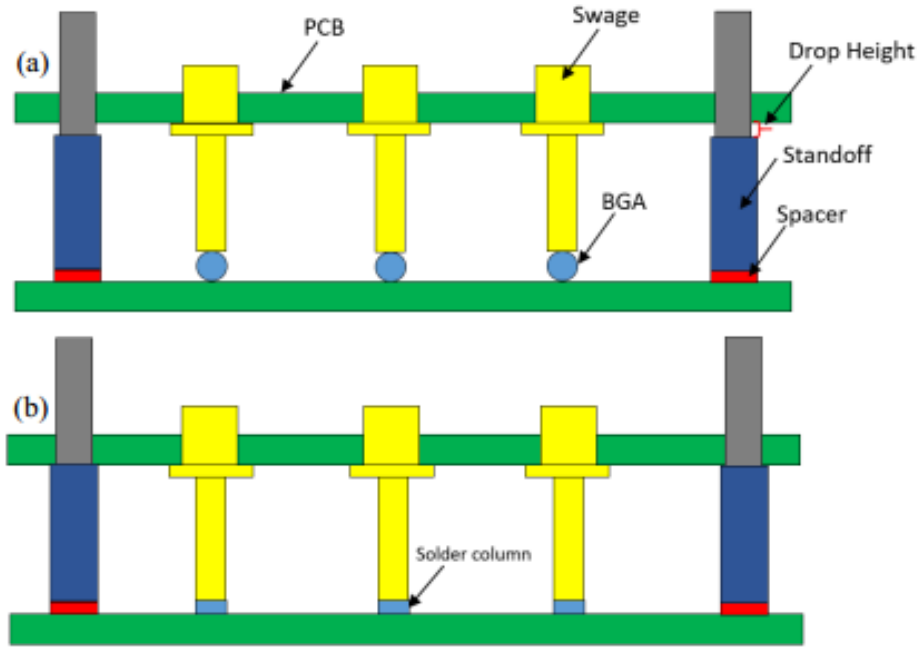

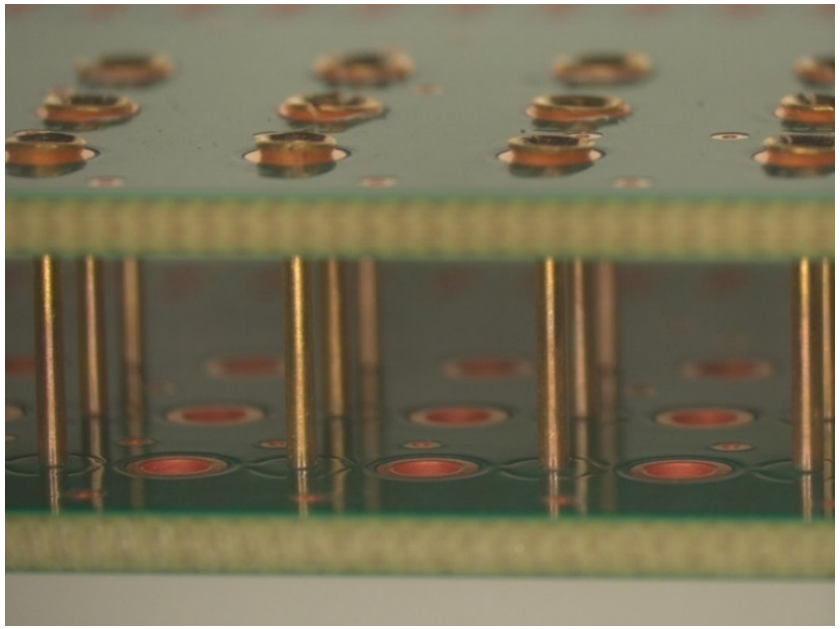

Redesigned Coupon: Assembly

- New interposer brass pins with swage interlock.
- Positioning BGA solder spheres in tacky flux.
- Faster construction procedure.
- BGA ball diameter and drop height to control final geometry of solder joints.
- Simplified geometry – uniform stress distribution

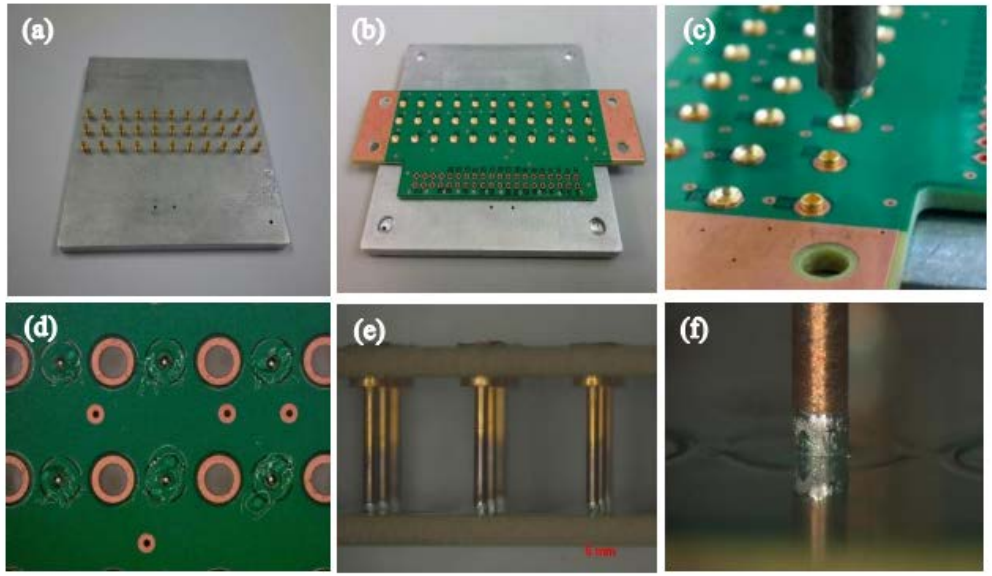

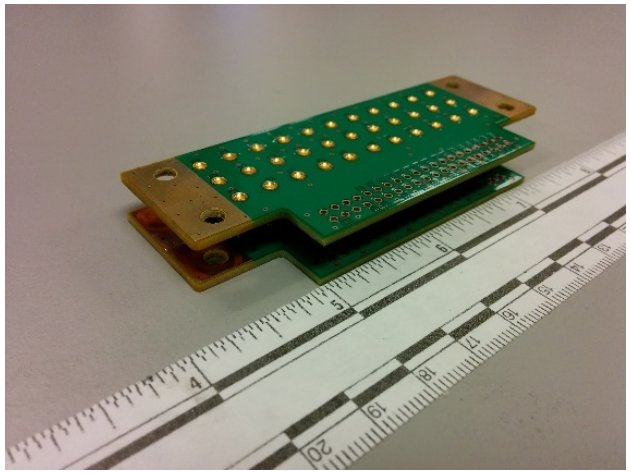

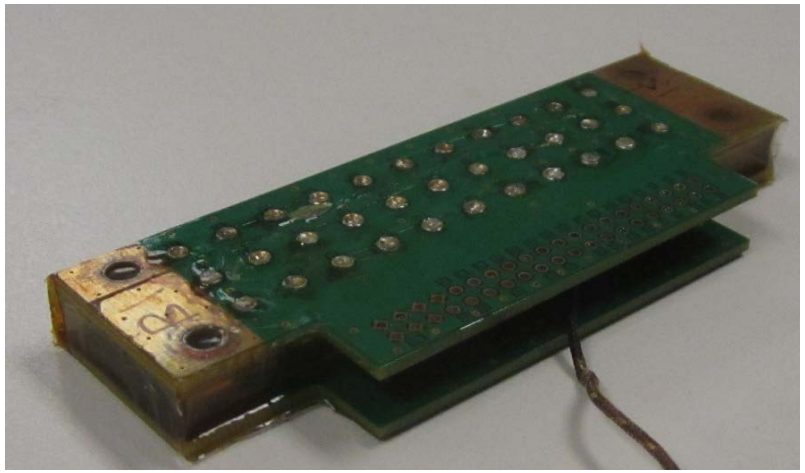

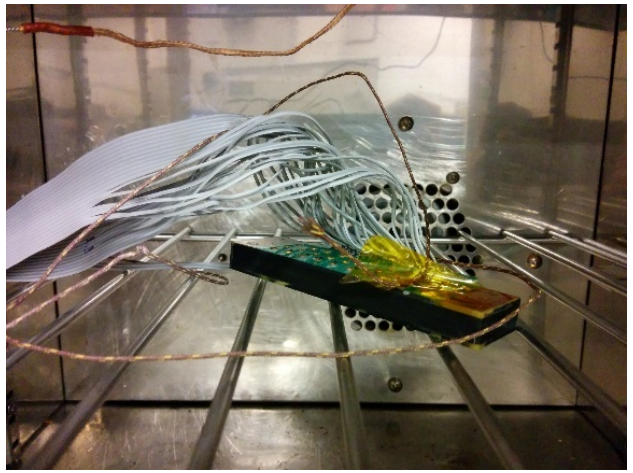

Material Selection

- Six potting materials used at different temperature profiles to vary the stress and strain levels induced on solder joints
- TMA and DMA characterization of modulus and CTE with temperature to determine exact transition of CTE and modulus.

Material ID	PM1	PM2	PM3	PM4	PM5	PM6
E (GPa)	1.02	2.81	0.16	0.34	10.7	2.5
T_g (°C)	35	145	-50	-2	130	120
CTE<T_g (ppm/°C)	77	37	N/A	N/A	28	44
CTE>T_g (ppm/°C)	195	N/A	340	87	83	N/A
Shore Hardness	84D	90D	56A	88A	91D	89D

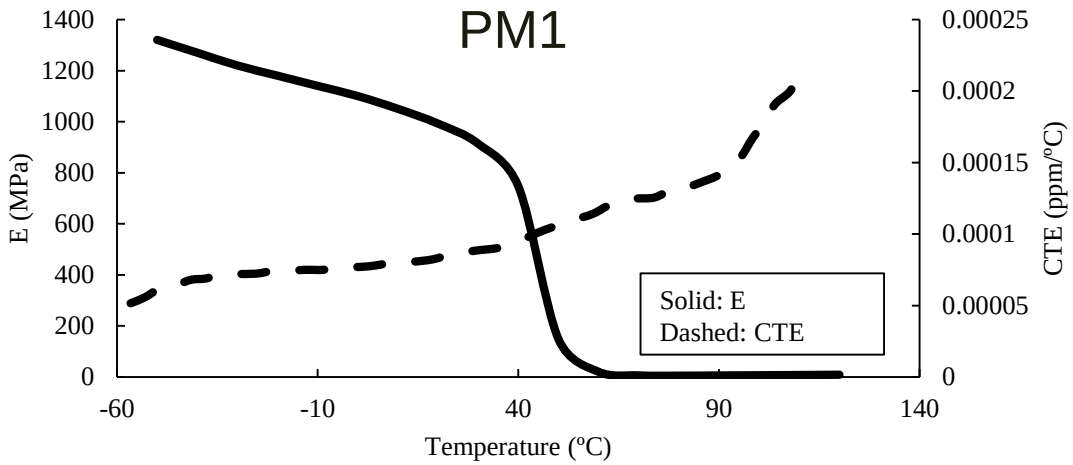

Thermal Cycling

- Temperature cycling of specimens at various temperature profiles
- Positive mean temperature will induce positive mean strain in solder joints
- Adjusting the mean temperature and temperature range to control peak and mean strain by controlling expansion rate of potting materials

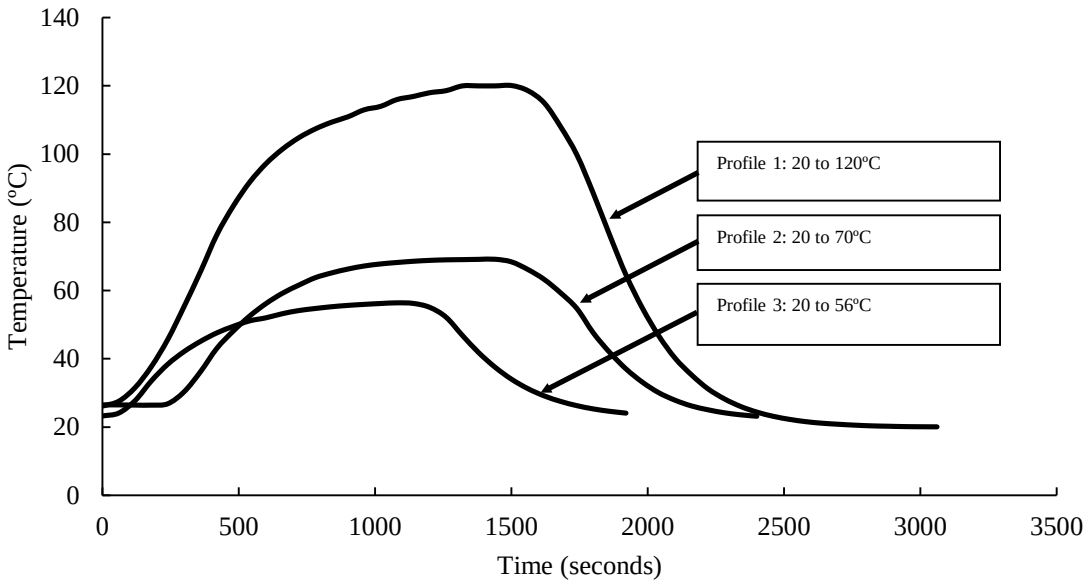

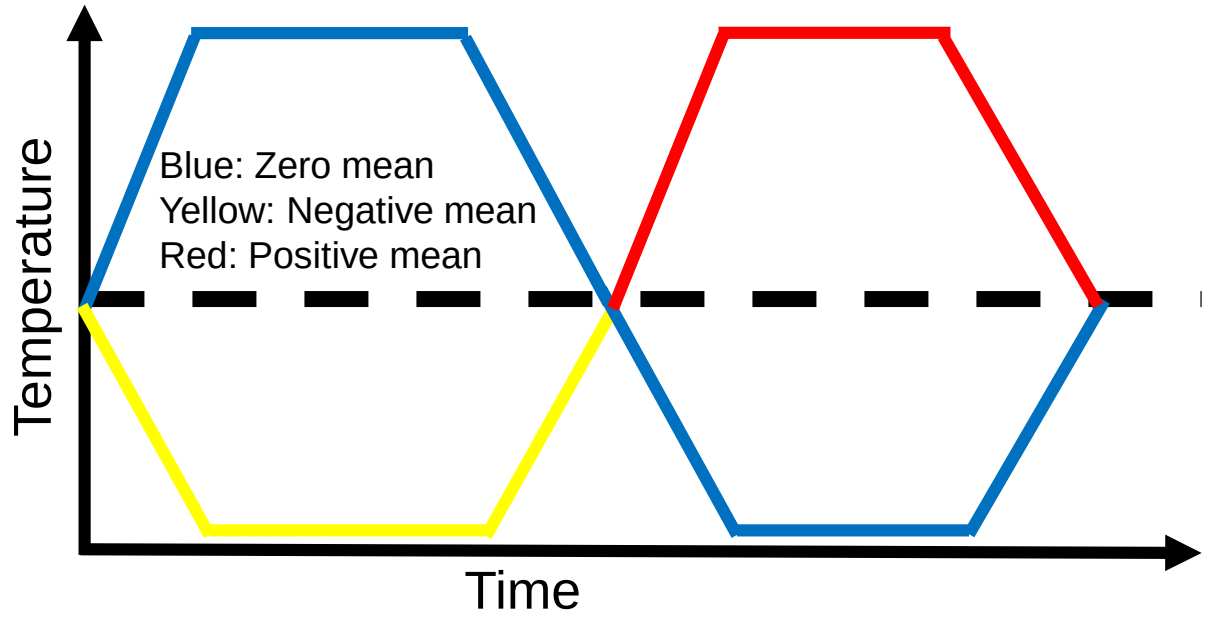

Experimental Results: Failure Mode

- Specimens assembled with solder stencil resulted in inconsistent solder joint geometry and volume. Large voiding in joints made with 8 mil thick stencil.
- Hourglass solder joints formation leading to indeterminate failure location.

Specimen ID	Solder Type	Solder Height	Temp cycle	Potting CTE	Failed	DNF	Beta	Eta	Total Cycles
B4	Stencil	200	-6 to 46	44	32	1	1.9	181	958

Cycles to failure and location in specimen

578	229	102	68	186	153	266	127	94	153	297
85	119	162	85	69	34	76	416	273	68	315
136	85	96	94	102	42	146	93	169	288	DNF

Connector side

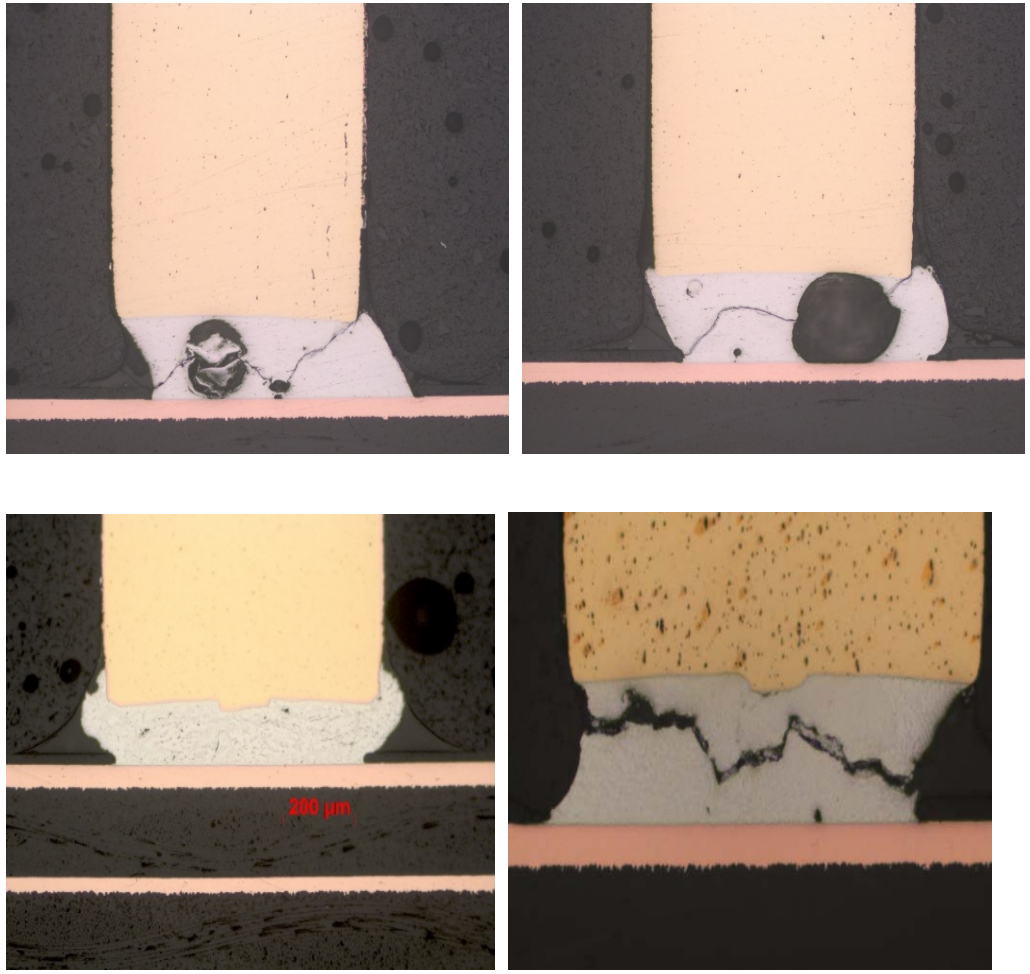

Experimental Results: Failure Mode

- Specimen with BGA solder joints
- Cracks propagate along the diagonal or along the top solder-brass pin interface at the bulk of the solder
- Shear band formation at interface due to large compressive plastic deformation

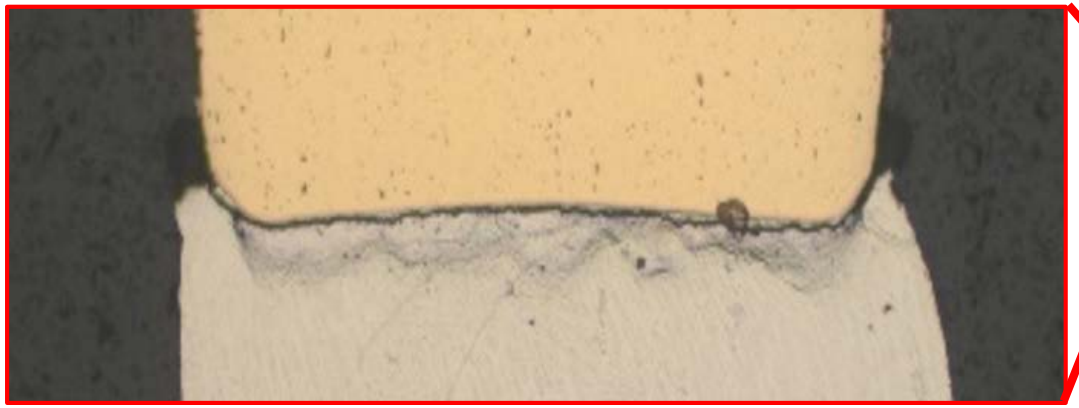

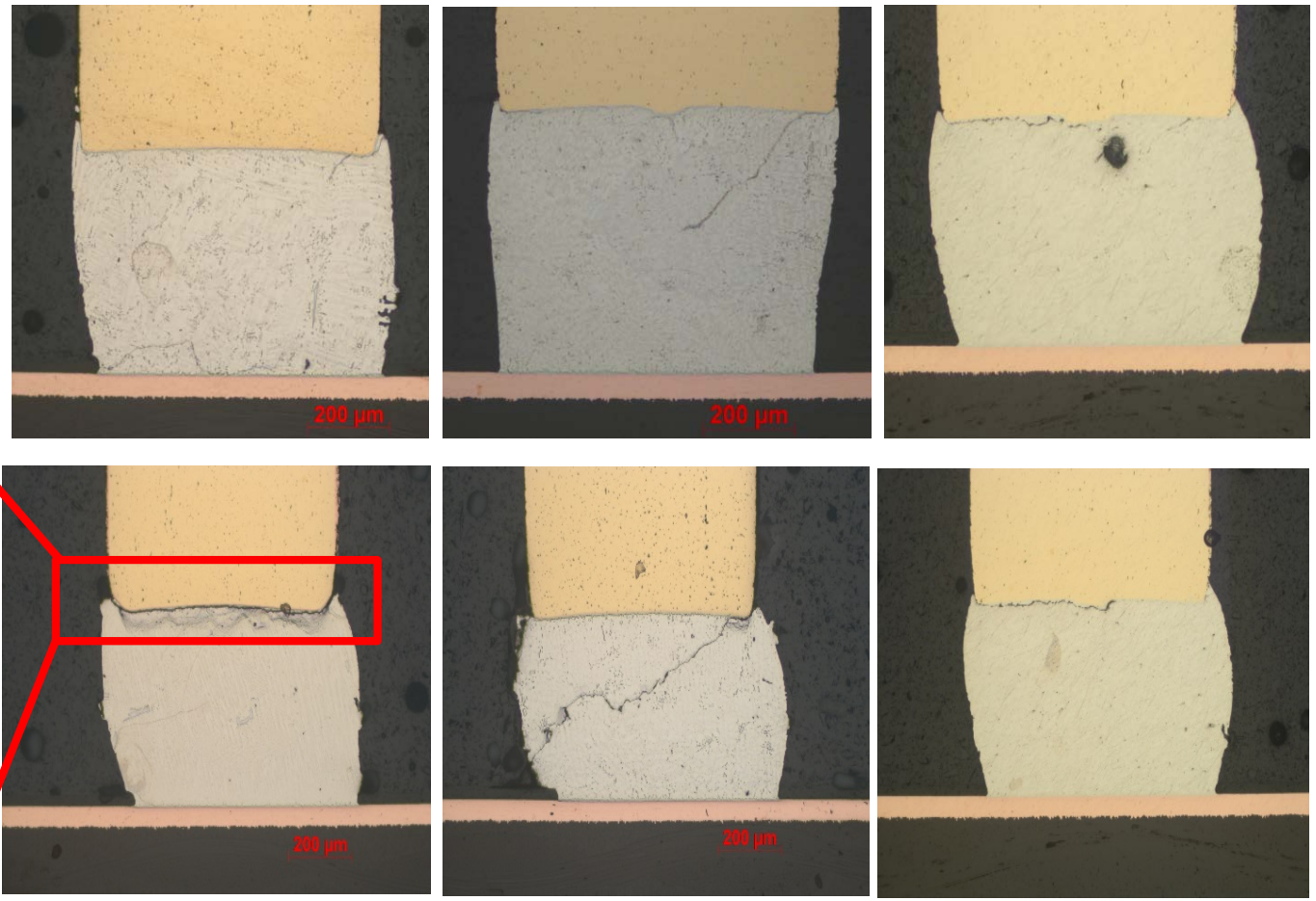

Experimental Results: Failure Mode

- Specimen cycled for 2000 thermal cycles from 20°C to 47°C. Potting material used with CTE of 44 ppm/ °C, E of 2.5 GPa and Tg of 120°C.
- Electrical continuity measurements during test to detect failures.
- Eta of 2367 Beta of 1.09.
- 17 recorded failures, 16 joints did not show electrical discontinuity.

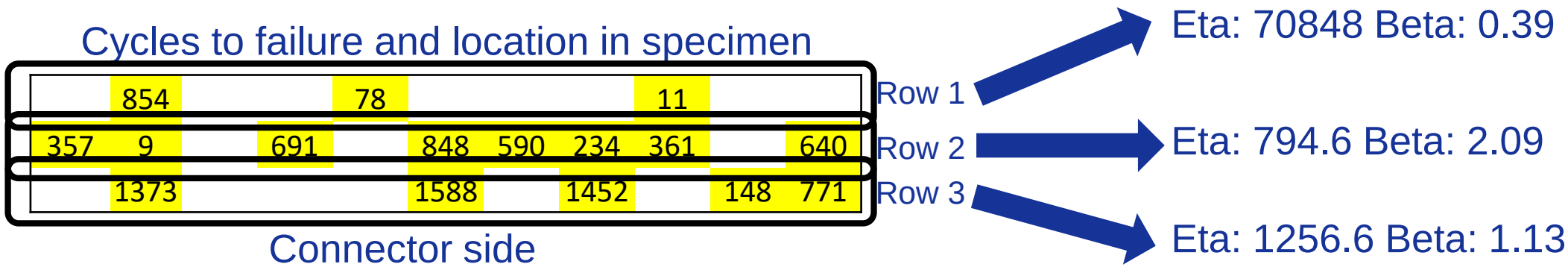

- Row 1
- Polarized light images

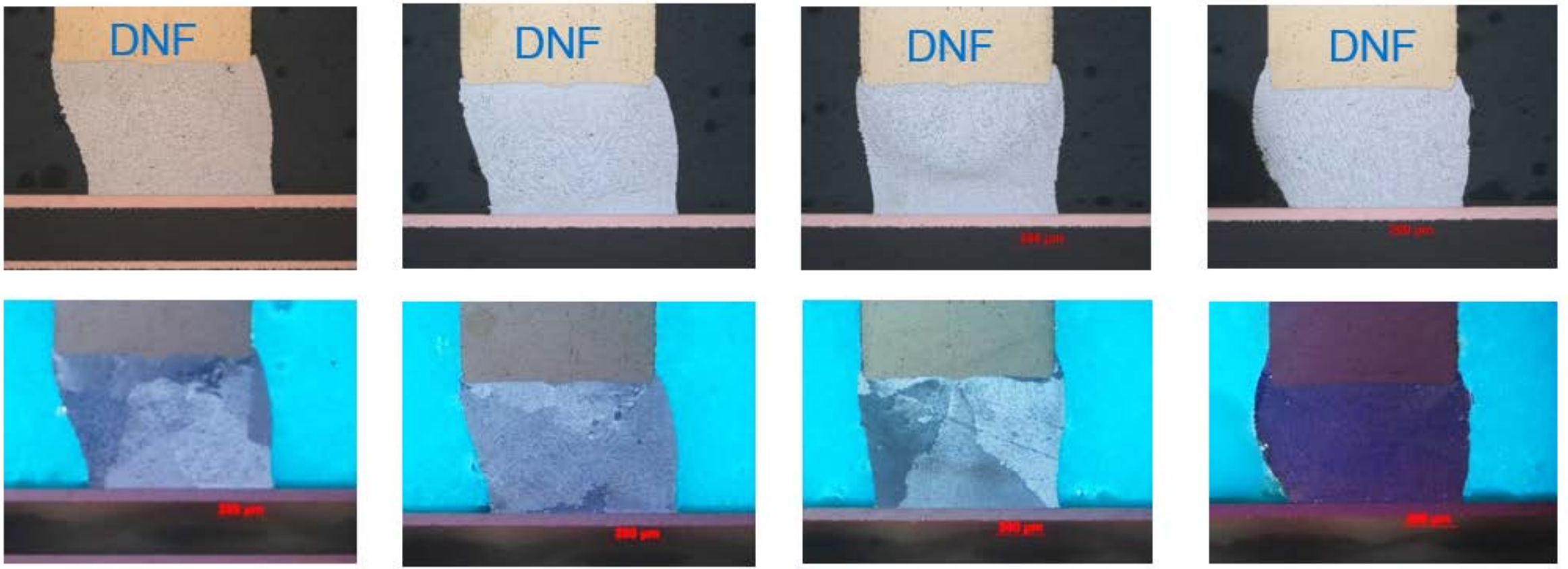

- Row 2
- Polarized light images

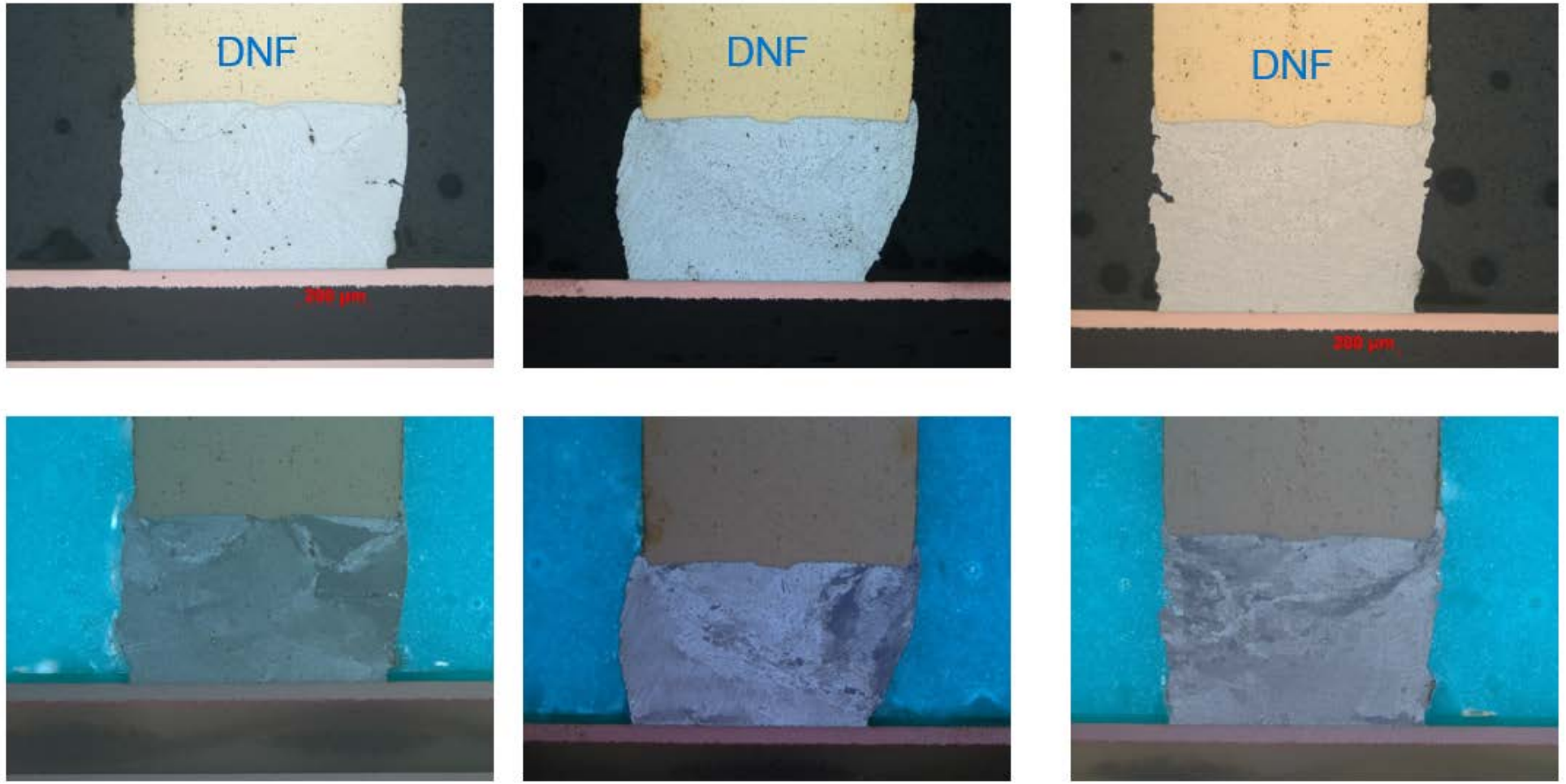

- Row 3

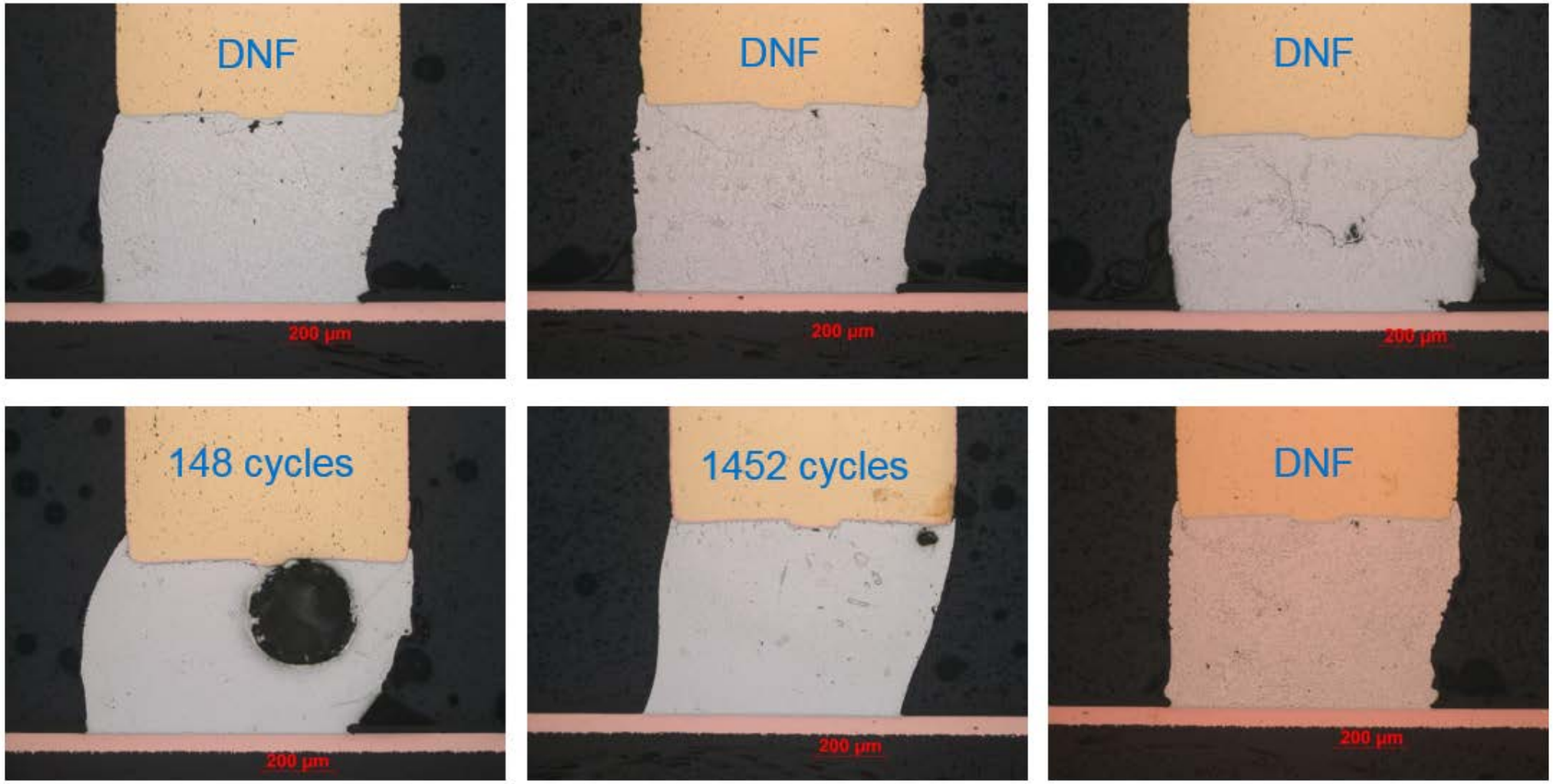
DNF
200 µm
DNF
200 µm
DNF
200 µm
148 cycles
200 µm
1452 cycles
200 µm
DNF
200 µm

Modeling: Analytical Approach

- Displacement compatibility calculation of axial stresses due to mismatch between potting material and solder alloy.
- Does not consider disparity between potting and solder lengths in loading direction.
- Assuming thermal stability of CTE and E through thermal loading.

$$F = \frac{\Delta T(\alpha_2 - \alpha_1)}{\left(\frac{1}{A_1 E_1} + \frac{1}{A_2 E_2}\right)}$$

Materials with constant CTE & E across temperature

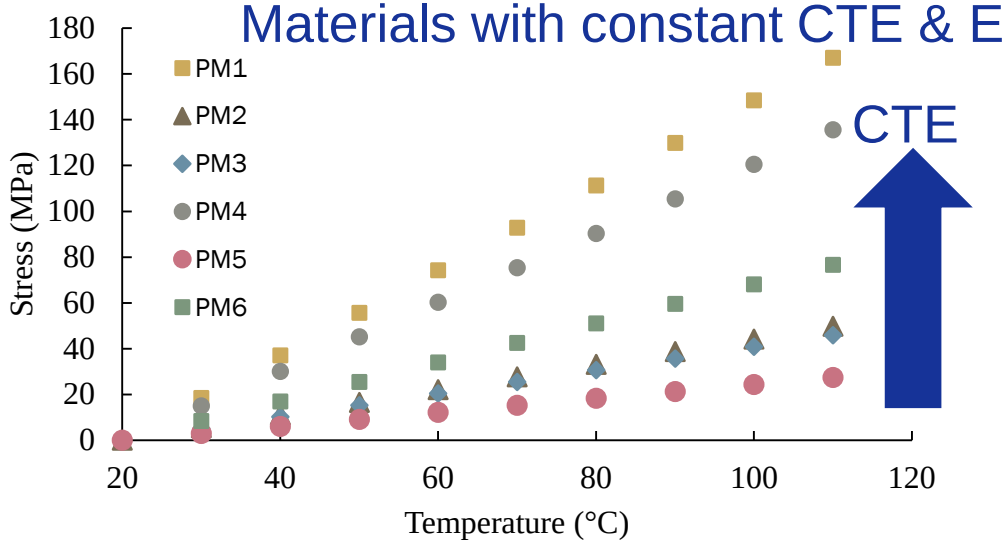

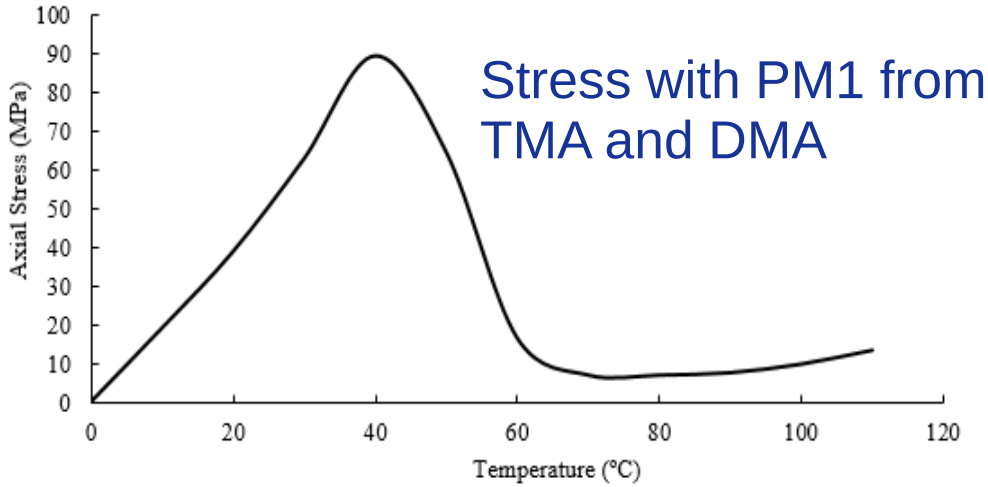

Modeling: Finite Element Analysis

- Production FE software model with creep constitutive model for SAC305 solder alloy.
- Assuming no interaction between potting material and pins.
- Global and local modeling approach.

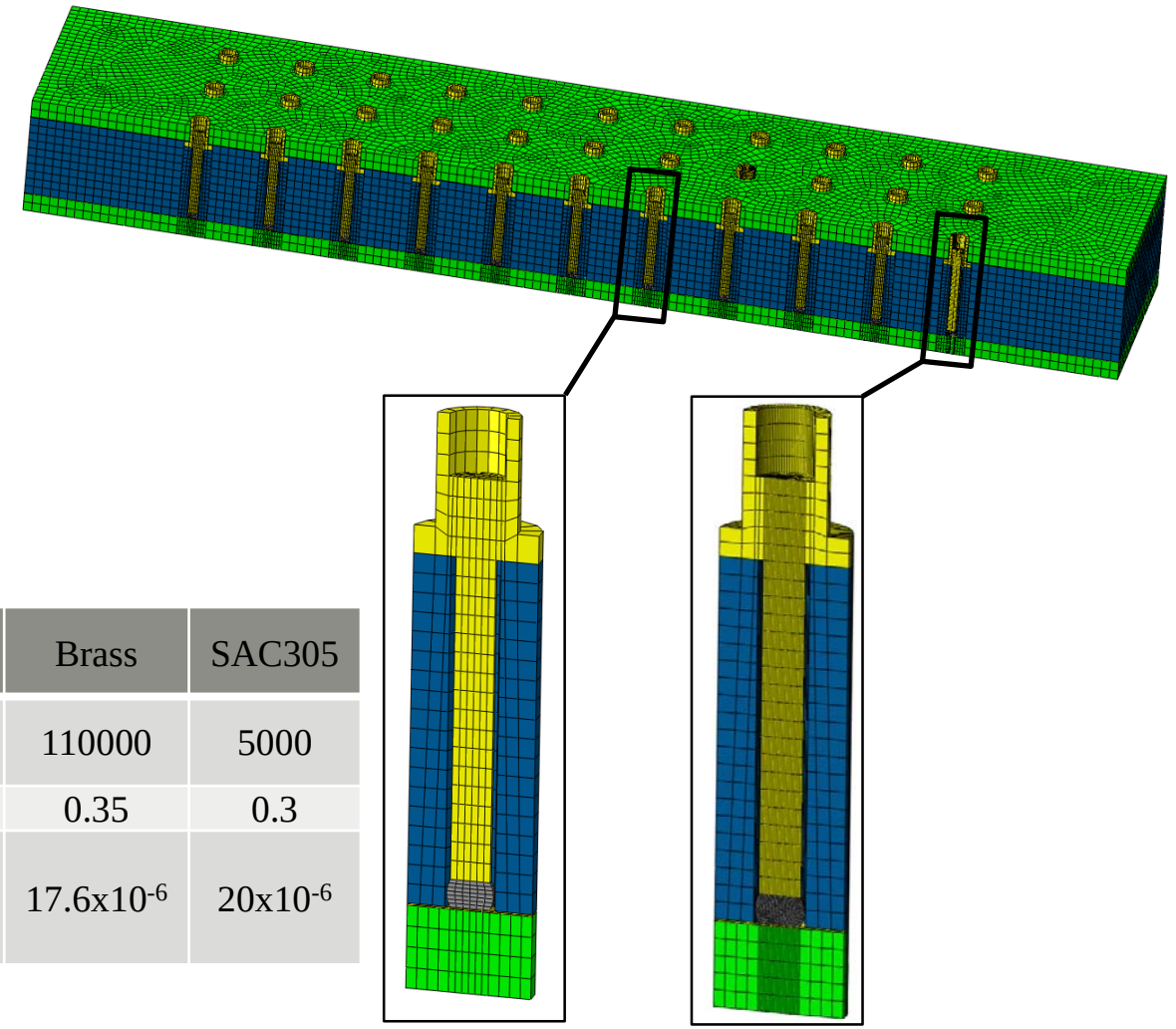

$$\dot{\varepsilon}^{cr} = A_1(sinh\alpha\sigma)^n \exp\left(-\frac{H_1}{kT}\right)$$

A_1	α	n	H_1	k
277984	0.02447	6.41	54041	8.314

Materials	PCB	Copper	Brass	SAC305
E (MPa)	33986	118590	110000	5000
v	0.13	0.326	0.35	0.3
CTE (ppm/°c)	16.9×10^{-6}	16.7×10^{-6}	17.6×10^{-6}	20×10^{-6}

Modeling: Finite Element Analysis

- Von Mises stress plot in (a) center joint (b) corner joint in specimen with PM2 at the end of high temperature dwell. Temp profile 2 (20 to 70°C)

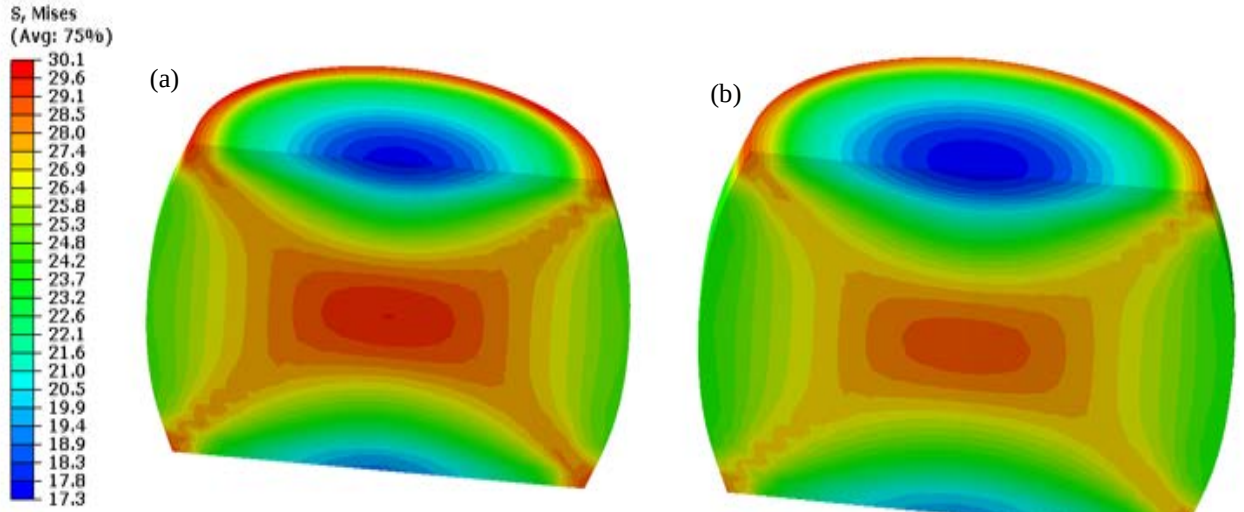

- Axial stress plot in (a) center joint (b) corner joint in specimen with PM2 at the end of high temperature dwell. Temp profile 2 (20 to 70°C)

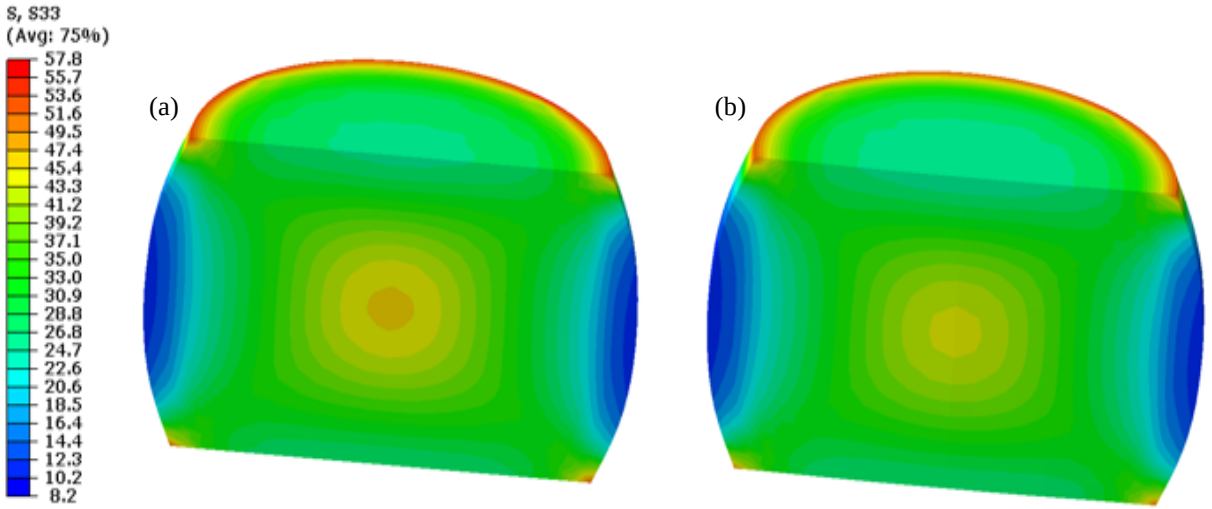

Modeling: Finite Element Analysis

- Accumulated creep strain energy density plot in (a) center joint (b) corner joint in specimen with PM6 with temperature profile 3 (20 to 56°C).
- Higher strain energy density is observed in joints at the center of the specimen due to larger axial strains.
- Corner joints posses slightly lower axial strain with more shear strain due to bending near edge of specimen.

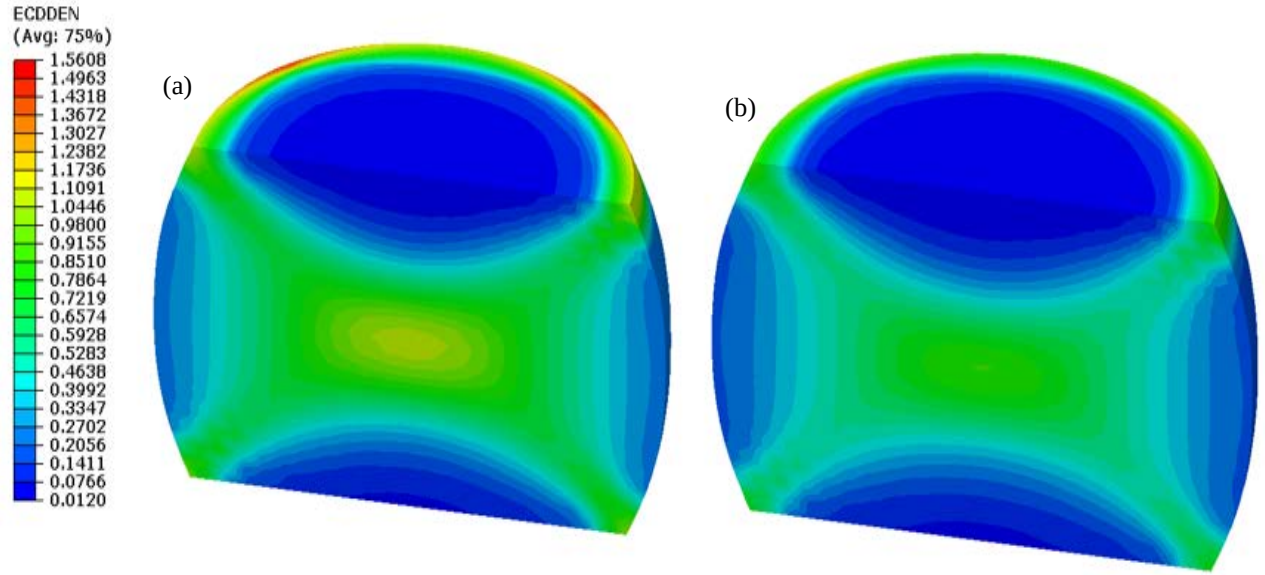

Modeling: Finite Element Analysis

- FE modeling correlates the damage location of tested solder joints under axial loading. Crack initiation and propagation agrees with location obtained from simulation results and explains diagonal crack growth pattern.

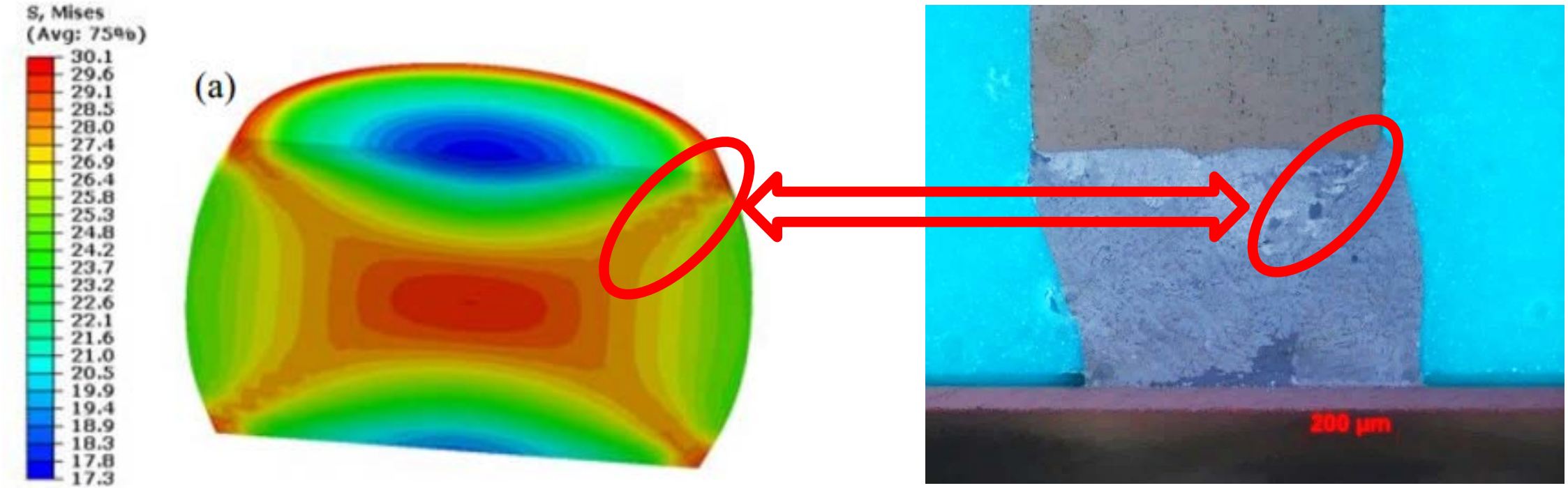

Modeling: Finite Element Analysis

- Displacement control of solder joint strain due to thermal expansion of potting material
- Stress amplitude does not deviate as much as strain range between the various potting materials
- Peak strain coincides with peak temperature, peak stress occurs prior due to potting expansion followed by relaxation until peak strain is achieved.

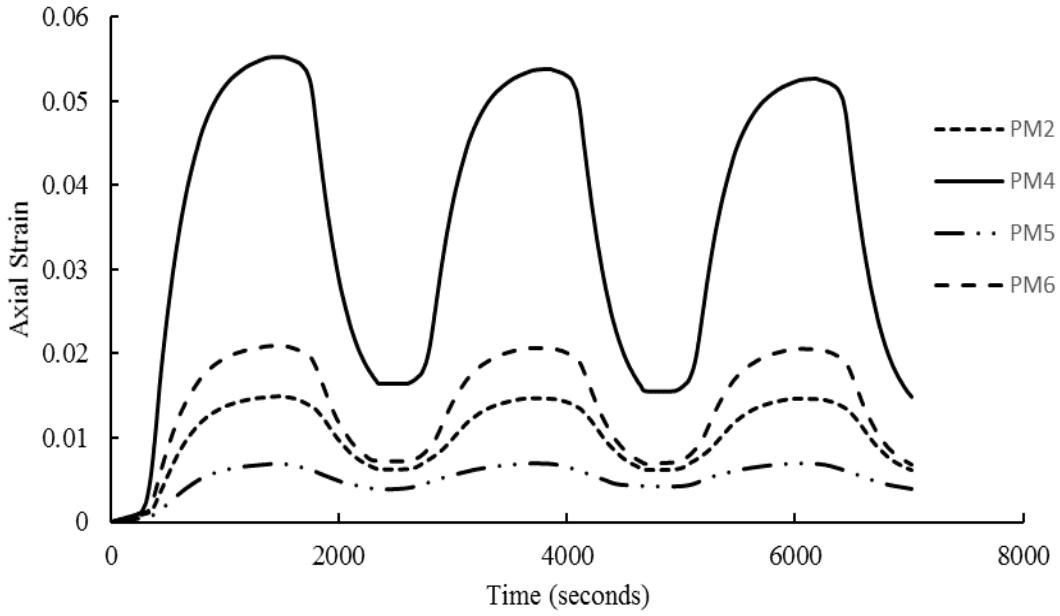

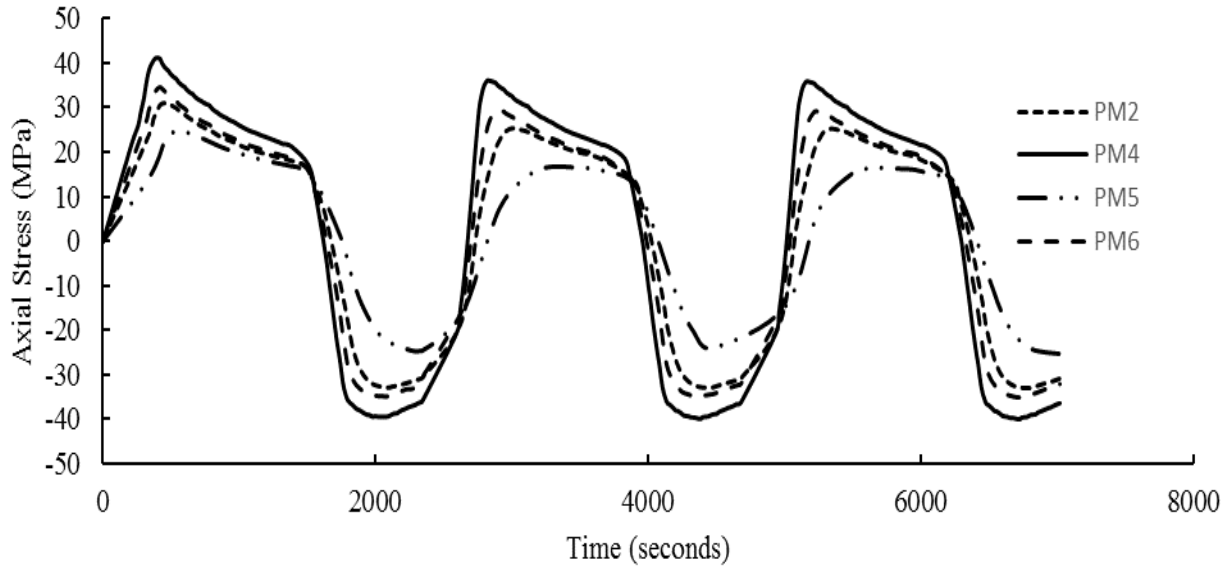

Modeling: Finite Element Analysis

- Strain-time behavior of two potting materials exhibits potting materials with low elastic modulus (rubber like) and high CTE apply significantly more axial strain than potting compounds with underfill characteristics at equivalent temperatures.
- Overstress failure was observed in specimens with PM4 under temperature profile 2. No failure was observed in specimens with PM5 under profile 1 past 2000 thermal cycles.

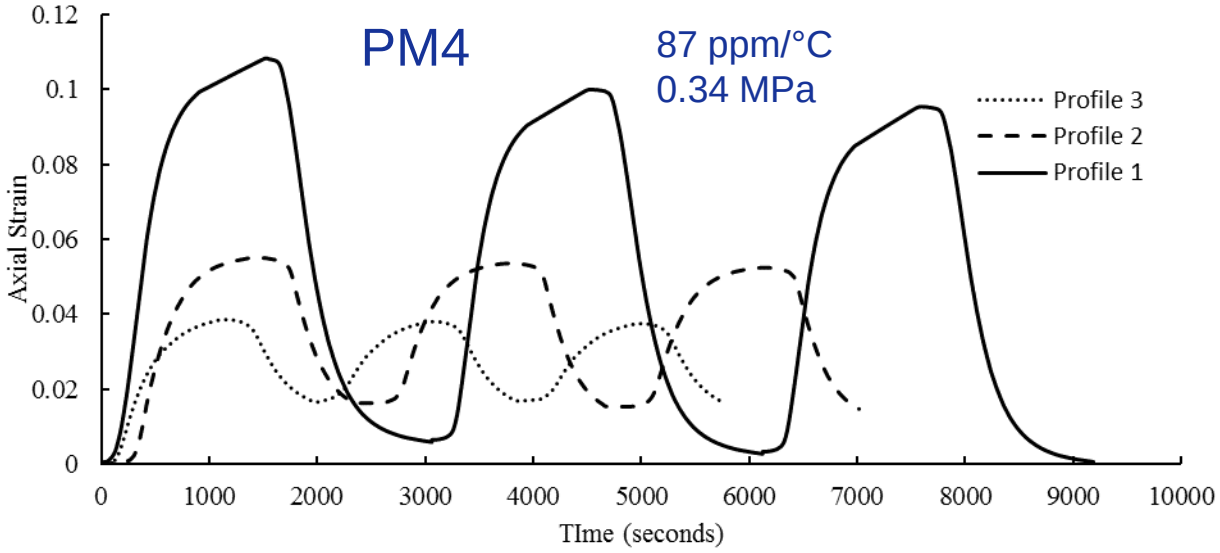

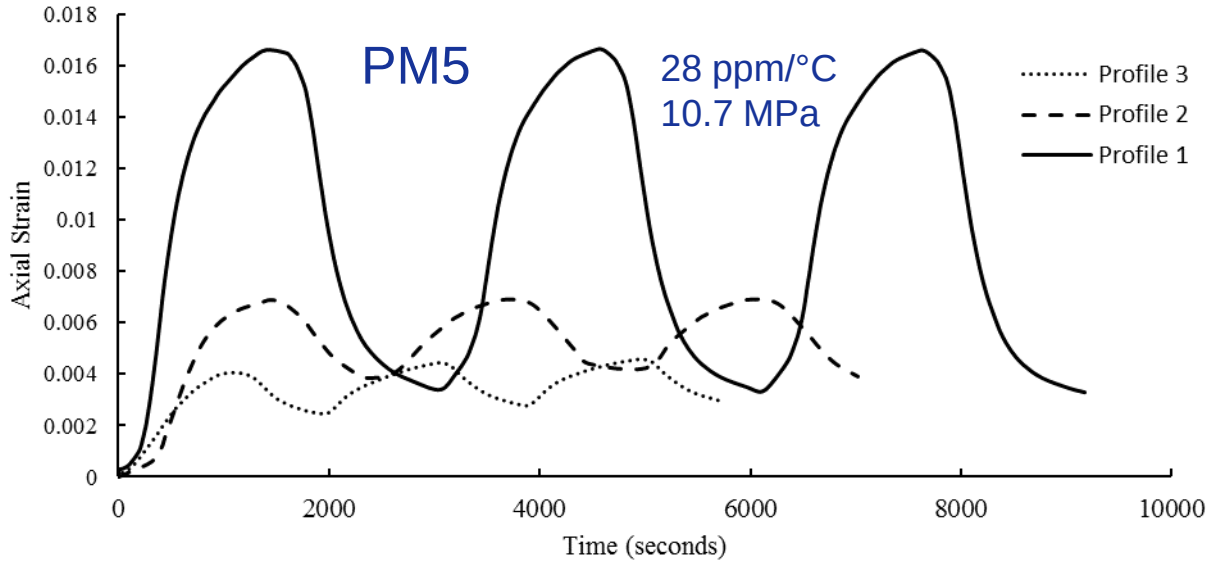

Conclusion and Future Work

- Fatigue life of BGA solder joints under purely axial loading is particularly sensitive to alignment of the joint geometry with respect to orientation of applied load.
- Analytical displacement compatibility does not account for solder joint and potting material height and fails to correlate to actual stress level experienced by solder joints.
- Stress distribution in BGA solder joints under axial loading experience maximum strain at the interface and flows into the bulk of the solder in a diagonal shape.
- FE modeling has been showed to correlate to region of damage accumulation in tested solder joints under axial loading.
- Current experiments are being conducted at various temperature profiles with different potting materials to distinguish the amount of damage under tensile and compressive axial loading.

Thank you for your attention!!

Questions?